SEQUESTRATION OF CO_2 BY CHEMICALLY REACTIVE AQUEOUS K_2CO_3 IN

HIGH EFFICIENCY ADSORBENTS USING MICROFIBROUS MEDIA

ENTRAPPED SUPPORT PARTICULATES

Except where reference is made to the work of others, the work described in this thesis is my own or was done in collaboration with my advisory committee. This thesis does not include proprietary or classified information.

_____

Noppadon Sathitsuksanoh

Certificate of Approval:

_____	_____
Robert P. Chambers Professor Chemical Engineering	Bruce J. Tatarchuk, Chair Professor Chemical Engineering
_____	_____
Gopal A. Krishnagopalan Professor Chemical Engineering	Joe F. Pittman Interim Dean Graduate School

SEQUESTRATION OF CO_2 BY CHEMICALLY REACTIVE AQUEOUS K_2CO_3 IN HIGH EFFICIENCY ADSORBENTS USING MICROFIBROUS MEDIA ENTRAPPED SUPPORT PARTICULATES

Noppadon Sathitsuksanoh

A Thesis

Submitted to

the Graduate Faculty of

Auburn University

in Partial Fulfillment of the

Requirements for the

Degree of

Master of Science

Auburn, Alabama
May 10, 2007

SEQUESTRATION OF CO_2 BY CHEMICALLY REACTIVE AQUEOUS K_2CO_3 IN HIGH EFFICIENCY ADSORBENTS USING MICROFIBROUS MEDIA ENTRAPPED SUPPORT PARTICULATES

Noppadon Sathitsuksanoh

_____
Signature of Author

_____
Date of Graduation

VITA

Noppadon Sathitsuksanoh, son of Thawat Sathitsuksanoh and Lawan Sae Koo, was born on January 28, 1980 in Bangkok, Thailand. He attended Chinorot High School and graduated in 1995. He enrolled in the Chemical Engineering program at Thammasat University in Bangkok, Thailand where he graduated with a Bachelors of Science in Chemical Engineering in May 1999 and then enrolled in Graduate School at Southern Illinois University shortly thereafter to pursue a Masters of Science in Mechanical Engineering. He graduated from Southern Illinois University with his Masters in May 2004. In August 2003, he enrolled in Graduate School at Auburn University.

THESIS ABSTRACT

SEQUESTRATION OF CO_2 BY CHEMICALLY REACTIVE AQUEOUS K_2CO_3 IN HIGH EFFICIENCY ADSORBENTS USING MICROFIBROUS MEDIA ENTRAPPED SUPPORT PARTICULATES

Noppadon Sathitsuksanoh

Master of Science, May 10, 2007
(B. S. ChE, Thammasat University, 1999)

123 Typed Pages

Directed by Bruce Tatarchuk

This work is mainly focused on developing a new adsorptive material and regenerable system for CO_2 removal to supply CO_2-free gas stream for low temperature and low CO_2 concentration applications, such as Alkaline Fuel Cells, Metal-Air batteries, and portable air-purifying respirators. A novel microfibrous media has been introduced for CO_2 filtration from wet gas streams at room temperature. The microfibrous media was prepared by uniformly dispersing activated carbon particulates in the nickel fiber matrix via wet layer paper-making/sintering processes. The use of microfibrous media in a composite bed maximizes the breakthrough capacity per unit volume and promotes high accessibility. The microfibrous media synergically combines the high contacting efficiency of the microfibrous matrix and the small internal mass transfer resistance of the small particulates. The capacity of the microfibrous media can be reversibly

recovered. The incorporation of microfibrous media to the Sodalime was observed. The result shows 120% improvement in the breakthrough capacity compared with the packed bed of the Sodalime with the same volume. This approach can be applied to miniaturize the reactor size, reduce thermal mass, and enhance the process intensification.

ACKNOWLEDGEMENTS

The author would like to thank the Sathitsuksanoh family; my mother, Lawan who has always been there for me; my sister, Varisa who encouraged me not to give in to my obstacles; my father, Thawat who always believes in me. I would like to also give the deepest thanks to my advisor, Dr. Bruce Tatarchuk who provided support and guidance throughout the learning processes. He allowed me to have freedom to learn more than course works could ever teach.

In addition, I would like to thank the following:

- Drs. Don Cahela and Yong Lu for their interesting discussions and advices throughout my course of study
- Hongyun Yang for his helps and suggestions in completing this research
- Drs. Robert Chamber and Gopal Krishnagopalan for taking the time to be on my thesis committee.

Style Manual Used: Chemical Engineering Progress Style Guide, available at www.cepmagazine.org/editorial/refstyle.htm

Computer Software Used: Microsoft Word, Microsoft Excel, Adobe Photoshop, Microsoft Visio, Win-Transfer

TABLE OF CONTENTS

LIST OF TABLES

LIST OF FIGURES

I. INTRODUCTION

Carbon dioxide sequestration has been of interest as the increment of CO_2 emissions contributes to the global warming and climate change [1]. Carbon dioxide is a product from many sources, such as human activities, vehicle emissions, and combustion in power plants. To develop a material for carbon dioxide control, a basic understanding of the individual system and the chemistry behind the system is needed.

There are a number of techniques that have been used to remove CO_2, such as Rectisol process, Selexol process, adsorption by solid sorbents, and absorption by liquid solvents. Such processes might be suitable for one application, but not another. Monoethanolaine (MEA) and hot potassium carbonate (K_2CO_3), for example, are often used in recovery of CO_2 in the ammonia industries, oil refineries, and petrochemical plants [2], both of which have high CO_2 removal capacity and efficiency. The same method can not be applied for scrubbing CO_2 in fuel cells for portable electronic devices or in space cabin or submarines due to the large unit size and zero gravity limitation. An alternative, such as a use of solid sorbents and membrane processes has been of interest to overcome these disadvantages. The membrane processes are effective, but costly due to the high pressure required inside the membrane reactors to allow the gas or liquid to

permeate through the membrane. In the case of solid sorbents, CaO is one of the most common carbon dioxide removal sorbents in power stations and coal gasification.

However, the reaction between CaO and CO_2 is a slow reaction at room temperature. As a result, CaO is usually operated at 500-600^{o}C. Molecular sieves often known as drying agents due to their moisture adsorption capacity by means of physical adsorption are often used to adsorb carbon dioxide in medical applications, such as during low-flow sevoflurane anaesthesia [3]. However, due to the high water adsorption, many beds of molecular sieves or silica are often incorporated in order to remove moisture prior to adsorption of carbon dioxide.

In this study, the combination of the liquid phase absorption and gas phase adsorption has been used to remove CO_2 from the wet gas stream at room temperature. The goal of this research is to synthesize a new carbon dioxide adsorbent that work at room temperature with regeneration capability and thermal stability. Many sorbents are considered in this study, such as Molecular sieves (3A, 4A, 5A, and 13X), CaO, Sodalime, potassium superoxide, and potassium carbonate. Energy dispersive x-ray spectroscopy, scanning electron microscopy, differential scanning calorimetry and x-ray diffraction are employed to examine chemical and structural changes of sorbents before and after breakthrough tests.

II. LITERATURE REVIEWS

A development of the greenhouse gas control technology has attracted much interest due to the concern of the possibility of global warming induced by the atmospheric accumulation of greenhouse gases. The current average carbon dioxide level has increased during the past century as shown in Figure 1 [4]. Carbon dioxide comes from many sources including the respiration processes of living; man-made sources of carbon dioxide come mainly from the burning of various fossil fuels for power generation and transport use, all of which induced an increase in greenhouse gases that is the cause of global warming.

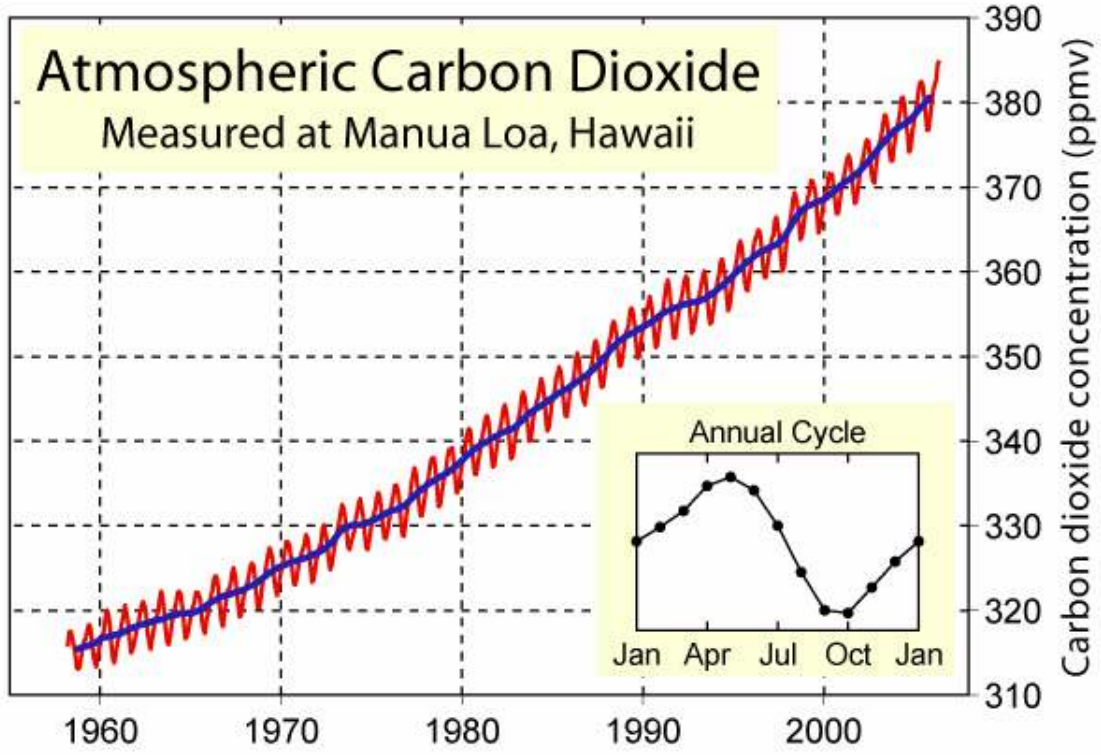

Figure 1: Atmospheric CO_2 concentrations in parts per million by volume, ppm, at Mauna Loa, Hawaii

Some combustion applications release a large quantity of carbon dioxide, which needs to be removed prior to storage or being released into atmosphere such as coal gasification, fossil fuel power plants, and syngas production [5,6]. As a result, in recent years many carbon dioxide removal processes have been developed to meet the requirement of many applications as shown in Figure 2 [7].

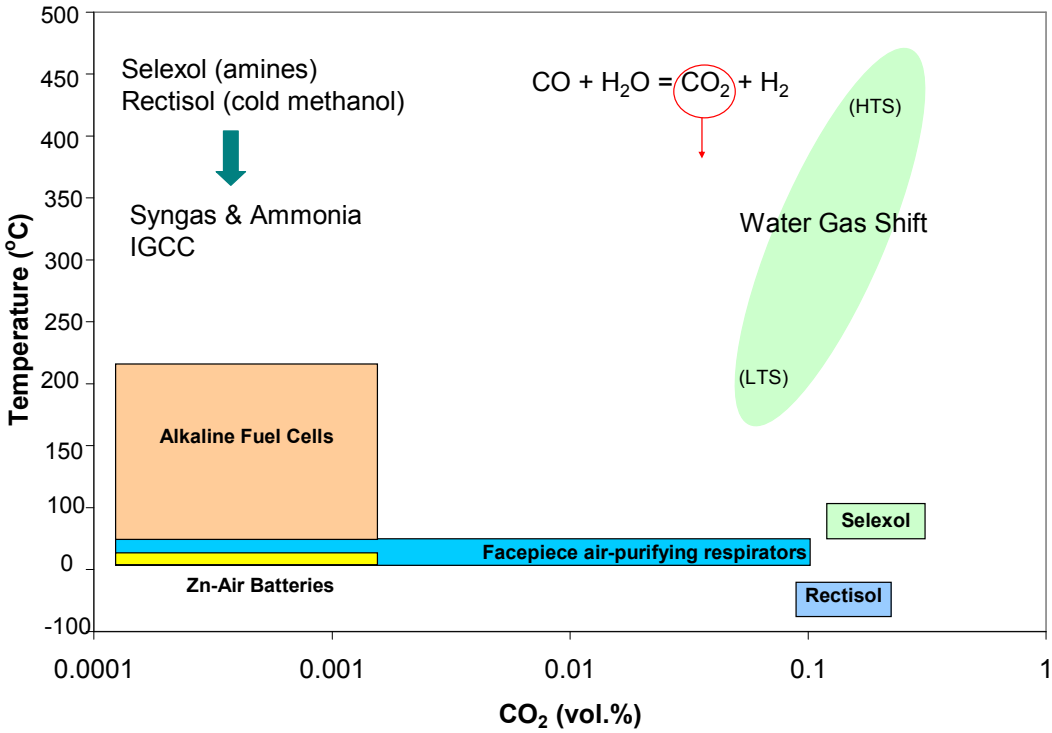

Figure 2: CO_2 concentration levels in selected applications

Applications of CO_2 Removal Processes

Fuel Cells and Batteries

The reformation of logistic fuels (i.e. JP8) involves many steps in order to obtain high purity hydrogen to power on-board Proton Exchange Membrane Fuel Cells (PEMFCs). Large amounts of carbon dioxide are obtained along the reformation and clean-up processes, which has to be reduced prior to entering the PEMFCs due to the possibility of side reactions, such as reverse water-gas shift, COS formation, or equipment corrosion [8,9]. Many technologies have been developed for CO_2 removal processes, such as

physical absorption, chemical absorption, adsorption, and membrane processes as shown in Table 1.

Table 1: Current CO_2 removal technologies

Technologies	Examples	Advantages	Disadvantages
Chemical absorption	• MEA (monoethanolamine) • DEA (diethanolamine) • MDEA (methyldiethanolamine)	• Low temperature operation (inlet gas can be around 40^{o}C)	• Corrosion by amines • Degradation of amines • CO_2 removal dependent on type of amines • Low heat efficiency
Physical absorption	• RECTISOL (cold methanol) • SELEXOL (dimethyl ether of polyethylene) • Sulfinol (mixture of • aqueous amine and sulfolane) • Fluor process (propylene carbonate)	• Low temperature operation (-70^{o} to 20^{o}C)	• High pressure operation • High capital cost • High energy consumption to maintain the solvents
Adsorption	• Alumina • Zeolite • Activated carbon	• Ease of use and storage	• Usually use for trace contamination • May require landfilling
Membrane processes	• Inorganic membrane (zeolite) • Polymeric membranes (microporous) - Polypropylene - Polyphenyleneoxide - Polydimethylsiloxane	• Ease of use • Compact equipment size	• Expensive • Low regeneration rate • Often required pre-treatment

Fuel Cells have been around for over 150 years, but it was in 1960s when the potential of fuel cells was recognized after NASA demonstrated in Space Shuttle Program. The development of fuel cells was slow due to the technical barriers and high investment cost. To date, there are many types of fuel cells suitable for different applications. Table 2 shows a comparison of different types of fuel cell technologies and their applications. The major concern of fuel cells is mainly on economic competition with existing technologies. Among these fuel cells, Alkaline Fuel Cells offer highest efficiency and has been used since the mid-1960s by NASA in the Apollo and Space Shuttle Program due to their high efficiency, which allows the electricity to be generated nearly 70%. Figure 3 shows simple diagrams of different types of fuel cells and their operations. It is shown that for AFCs, high purity O_2 and H_2 are required to obtain high efficiency and extend the life of electrolyte (i.e. KOH) from poisoning. As a result, AFCs are very costly; mainly due to the operational costs from frequent replacement of CO_2 scrubbers to maintain high purity H_2 and O_2. Carbon dioxide can be used to generate water once separated from air in Bosch and Sabatier processes [10], which is one of the main reasons this type of fuel cells is used mainly under Life Support Program (LSS) in military and space programs.

Table 2: Comparison of Fuel Cell Technologies [11]

Fuel Cell Type	Common Electrolyte	Operating T.(°C)	System Output	Efficiency	Applications	Advantages	Disadvantages
Polymer Electrolyte Membrane (PEM)	Solid organic polymer polyperflu-orosulfonic acid generation	50-100	<1kW-250kW	50-60% electric	- Back-up power - Portable power - Transportation	- Solid electrolyte reduces corrosion & electrolyte management problem - Quick start-up - Low temperature	- Expensive catalysts - Sensitive to impurities - Low temperature waste heat
Alkaline (AFC)	Aqueous solution of potassium hydroxide soaked in a matrix	90-100	10kW-100kW	60-70% electric	- Military - Space	- Cathode reaction is faster in alkaline electrolyte so high performance	- Expensive to remove CO_2 from fuel and air is required
Phosphoric (PAFC)	Liquid phosphoric acid soaked in a matrix	150-200	59kW-1MW (250kW module typical)	36-42% electric (80-85% overall with CHP)	- Distributed generation	- High efficiency - High tolerance to impurities in hydrogen - Suitable for CHP	- Pt catalyst - Low current and power - Large size/weight
Molten Carbonate (MCFC)	Liquid solution of lithium, sodium, and/or potassium carbonates, soaked in a matrix	600-700	<1kW-1MW (250kW module typical)	60% electric (85% overall with CHP)	- Electric utility - Large distributed generation	- High efficiency - Fuel flexibility - Variety of catalysts can be used - Suitable for CHP	- High temperature speeds corrosion and breakdown of cell components - Complex electrolyte management - Slow start-up
Solid Oxide (SOFC)	Solid zirconium oxide to which a small amount of yttitra is added	650-1000	5kW-3MW	60% electric (85% overall with CHP)	- Auxiliary power - Electric utility	- High efficiency - Fuel flexibility - Variety of catalysts can be used - Suitable for CHP - Solid electrolyte reduces electrolyte management problem - Suitable for CHP	- High temperature enhances corrosion and breakdown of cell components - Slow start-up

* CHP = Combined Heat and Power

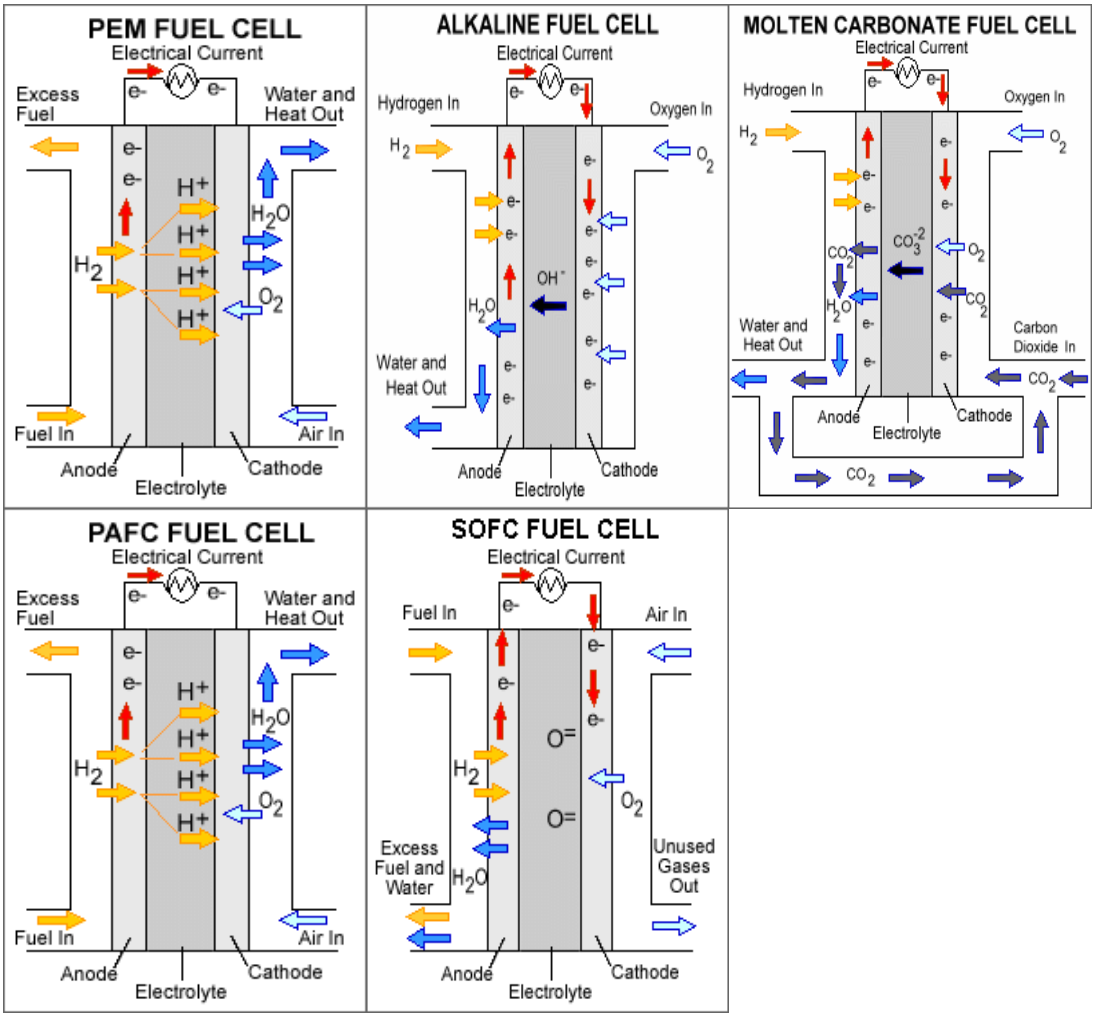

Figure 3: Basic configuration of different types of fuel cells

Zn-Air Batteries

Similar to Alkaline Fuel Cells, the use of liquid solvent to remove CO_2 is not viable in practice for Zn-air batteries. Zinc-air batteries, an example of metal-air batteries are energized only when atmospheric oxygen is absorbed into the electrolyte through a gas-permeable, liquid-tight membrane. They use the oxygen from air at the cathode as shown in the basic chemical reaction below [12].

At Air cathode: $0.5O_2 + H_2O + 2e^- \rightarrow 2OH^-$

At Zn anode: $Zn \rightarrow Zn^{2+} + 2e^-$

$Zn^{2+} + 2OH^- \rightarrow Zn(OH)_2$

$Zn(OH)_2 \rightarrow ZnO + H_2O$

Overall : $Zn + 0.5O_2 \rightarrow ZnO$ $\quad E^0 = 1{:}65V$

The basic configuration of the zinc-air batteries is shown in Figure 4.

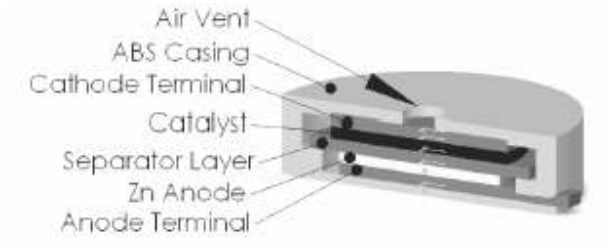

Figure 4: Cross-sectional view of the basic zinc-air batteries

Zn-Air batteries are often used in many portable applications, such as hearing aids, pagers, and mobile electronic devices. The essential components of a Zn-air cell are the negative terminal, anode, separator, cathode catalyst, cathode, positive terminal, and electrolyte. The electrolyte is typical potassium hydroxide utilizing OH^- as a charge carrier. Atmospheric oxygen is reduced at the cathode. The size of the air vent determines the energy density of the cell. However, zinc-air batteries are very sensitive to temperature, moisture and carbon dioxide from air. The carbon dioxide from air usually leaks through the membrane forming carbonate compound, which reduces the OH^-. The formation of this carbonate results in low conductivity and premature capacity reduction.

Among current CO_2 removal technologies, liquid phase absorption is not possible for this application due to the fact that it is not amendable for ransom orientation. As a result, many other sorption based technologies have been developed, such as molecular sieves, dolomite, LiOH, and potassium super oxide as shown in Table 3. Molecular sieves/zeolites are typically used to remove CO_2 via physical adsorption in the pore structure of the zeolites during anesthesia. The use of chemical compounds, such as Sodalime, Baralime, Carbolime, lithium hydroxide, potassium superoxide, and dolomite (CaO) causes a concern of the reaction between the sorbent and anesthetic.

Table 3: Selected currently available CO_2-sorbents

Liquid Solvents

Candidates	Amine (absorption)	K_2CO_3 $K_2CO_3+CO_2+H_2O=2KHCO_3$ (reaction)
Saturation Capacity g CO_2/g sorbent	0.0882 (PEI: polyethylenimine)	0.318
Regeneration Temp. (^oC)	150	180-250
Use	-IGCC power plants	- Ammonia and syngas production
Disadvantages	- Excess moisture increases ΔP and reduces capacity	- Liquid phase absorption - Large space required - Not readily amendable to random orientation

Solid Sorbents

Candidates	LiOH $2LiOH+CO_2=Li_2CO_3+H_2O$ (reaction)	Dolomite $CaO+CO_2=CaCO_3$ (reaction)	Potassium superoxide $2KO_2 + CO_2 = K_2CO_3 + 1.5O_2$ (reaction)	Molecular Sieves (adsorption)
Saturation Capacity g CO_2/g sorbent	0.920	0.786	0.31 plus 1.5 mol O_2 generated	0.066 (MS 5A)
Regeneration Temp. (^oC)	1310	600-900	>2000	250-350
Use	- AR Systems	-Coal gasification -IGCC plants	-AR systems (Drager®)	- Natural gas treat. - AFCs
Disadvantages	-High regen. T. -Short duration -One time use	- Kinetically slow at low temp. - High regen. T	- High regen. T - One time use	- Protective bed is needed to remove H_2O - Easy to degrade

Gasification

Today's most commercial CO_2 removal units for power industries utilize a chemical absorption of aqueous solvents due to their high CO_2 removal capacity and their ability to regenerate. However, the aqueous solvent units usually suffer from large unit size and their complexity from recycling spent solvents and maintaining the operating temperatures. Rectisol process, for example, has to maintain the temperature around -50^{o}C.

In the fossil fuel power plant, integrated gasification combined cycle (IGCC) power plants are considered very efficient and relatively clean. The natural gas field is found to contain at least 50% by volume [13]. With the combination of Rectisol or Selexol process, 50-60% energy conversion can be reached with "zero" CO_2 emissions [14-16]. However, these technologies are costly and high energy consumption. As a result, several other processes have been introduced into power plants, such as solid sorbents and membrane processes.

Membrane Processes

While membrane processes are usually light and compact, membranes usually operates at high partial pressure of CO_2 to ensure the permeability through the membrane, which causes high energy consumption. Moreover, the gas has to be relatively clean from small particulates to prevent the blockage from particles. The gas selectivity of the current

membrane technology is still inadequate. As a result, a large area of membranes is required to remove a small amount of CO_2.

Reforming

CaO has long been used for CO_2 removal associated with power stations and coal gasification [17]. Recently CaO has been used in steam reforming and water-gas shift to break the thermodynamic barrier by simultaneously removing CO_2 and thus pushes the reaction further towards H_2 production. This increases the production and purity of hydrogen, increases the CO conversion, and effectively removes carbon species from the gas phase product as shown in methane reforming in Figure 5.

Steam Reforming:	$CH_4 + H_2O \Leftrightarrow 3H_2 + CO$	$\delta H = 206$ kJ/mol
Water-gas shift:	$CO + H_2O \Leftrightarrow H_2 + CO_2$	$\delta H = -41$ kJ/mol
Overall:	$CH_4 + 2H_2O \Leftrightarrow 4H_2 + CO_2$	$\delta H = 165$ kJ/mol

A separated CO_2 product can be recovered from the adsorbent by regenerating the bed under reduced gas phase pressures, i.e. via pressure swing adsorption (PSA) concepts or temperature swing adsorption (TSA), which normally takes place around 800^oC. The advantages of combining the water-gas shift reaction with CO_2 adsorption is the high conversion since the equilibrium limited reaction is increased through the removal of a product of reaction.

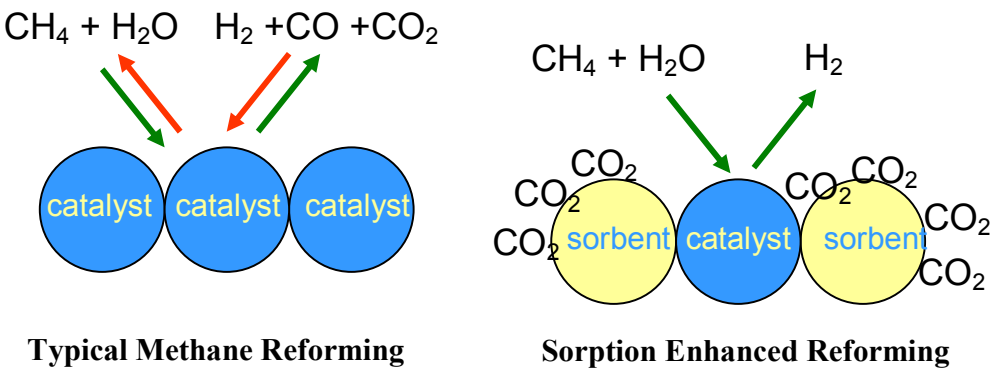

Figure 5: Adsorption enhanced catalytic processes

Other Low Carbon dioxide concentration Applications

The objective of this study is mainly focused on the low concentration carbon dioxide applications. The use of aqueous solvents is not plausible for such applications as mentioned. This is not only because of the fact that aqueous solvents are not amendable to random orientation, but also due to high operating cost, large unit size, low heat efficiency, solvent degradation, and equipment corrosion. Thus, the development of a new material for a cost-effective filtration with high CO_2 adsorption capacity is needed. The use of solid sorbents attracts much interest to overcome these disadvantages due to its low cost, low energy consumption, and wide range of operating temperatures and pressures. Moreover, the use of solid sorbents for adsorption combines with chemical reactions results in promoting reactions, which is normally limited by equilibrium such as steam reforming and water-gas shift. In case of waster gas shift reaction in IGCC processes, CO_2 removal process results in shifting the reaction toward lower CO concentration, generating more

hydrogen, which can be used for fuel cells. However, many solid sorbents usually require high regeneration temperatures, such as LiOH and dolomite compared to the liquid solvent counterparts.

Air-purifying Respirator

Many methods are employed for CO_2 removal from a close-circuit breathing apparatus in military and medical applications, such as the use of monoethaoamine, LiOH, and the recent KO_2. However, the use of potassium superoxide is one of the most interesting methods for breathing atmosphere. The reaction between KO_2 and CO_2 at 25^{o}C is as follows:

$2KO_2 + H_2O \rightarrow 2KOH + 1.5O_2$ $\delta H = 5.502$ kJ

$2KOH + CO_2 \rightarrow K_2CO_3 + H_2O$ $\delta H = -193.154$ kJ

$2KO_2 + CO_2 \rightarrow K_2CO_3 + 1.5O_2$ $\delta H = -187.652$ kJ

Based on the chemical reaction, it is shown that one mole of carbon dioxide reacts with two moles of potassium superoxide forming the emission of 1.5 mole of oxygen. However, the reaction is highly exothermic and the potassium superoxide is highly unstable. As a result, solid sorbents based on hydroxides of alkali metals is often used to remove CO_2 from the closed-circuit atmosphere, such as Baralime® and Sodalime®. The chemical composition of Baralime and Sodalime is shown in Table 4.

Table 4: Chemical composition of Baralime and Sodalime

Sorbents	Baralime	Sodalime
Chemical Composition	• 80% $Ca(OH)_2$ • 20% $Ba(OH)_2$	• 94% $Ca(OH)_2$ • 5% NaOH • 1% KOH

This type of sorbents is a mixture of $Ca(OH)_2$, and sodium-, potassium, and barium hydroxides. For reaction with carbon dioxide, water is rather necessary and the mixture of this type of sorbents usually contains 12-20% H_2O. Baralime demonstrated to have high carbon dioxide adsorption capacity; however, barium hydroxide is rather corrosive and the presence of potassium hydroxide causes degradation of anesthetic agent in medical applications.

Current packed-bed technologies for CO_2 recovery from flue gases utilize zeolites/molecular sieves for the pressure-swing adsorption in a dry gas stream. The flue gases usually contain 8-17% moisture, which affect the adsorption capacity of these solid sorbents. As a result, the moisture traps have to be used to remove moisture prior to removing carbon dioxide resulting in large adsorbers.

Molecular sieves are another type of sorbents that have been used for carbon dioxide control from the cabin air for space station by NASA [18]. This system utilizes a combination of silica and molecular sieve 13X to remove water vapor and molecular sieve 5A to remove carbon dioxide.

Molecular Sieves

Molecular sieves are crystalline metal aluminosilicates with interconnecting tetrahedral network of silica and alumina. The uniform cavities of the molecular sieves selectively adsorb molecules of a specific size. Table 5 shows some selected molecules and their critical diameters.

Table 5: Selected molecules and their critical diameters [19]

Molecule	**Critical diameter** (Å)
Helium	2.0
Hydrogen	2.4
Acetylene	2.4
Oxygen	2.8
Carbon monoxide	2.8
Carbon dioxide	2.8
Nitrogen	3.0
Water	3.2
Ammonia	3.6
Hydrogen sulfide	3.6
Argon	3.8
Methane	4.0
Ethylene	4.2
Ethylene oxide	4.2
Ethane	4.4
Methanol	4.4
Methyl mercaptan	4.5
Propane	4.9
n-Butane to *n*-docosane	4.9
Propylene	5.0
Ethyl mercaptan	5.1
1-Butene	5.1
trans-2-Butene	5.1
1,3-Butadiene	5.2
Chlorodi fluoromethane (Freon 22®)	5.3
Thiophene	5.3
Isobutane to isodocosane	5.6
Cyclohexane	6.1
Benzene	6.7
Toluene	6.7
p-Xylene	6.7
Carbon tetrachloride	6.9
Chloroform	6.9
Neopentane	6.9
m-Xylene	7.1
o-Xylene	7.4
Triethylamine	8.4

A 4 to 8-mesh sieve is normally used in gas phase applications, while the 8 to 12-mesh type is common in liquid phase applications. The concept of the molecular sieves is to adsorb species smaller than the pore size of the molecular sieves. 3A molecular sieves have the effective pore size ~3A. As a result, 3A adsorbs species with diameter less than 3A, e.g. ethane.

Table 6: Properties of Selected Molecular sieves

Type	Composition	Pore size (A)	Adsorbed species
3A	0.6 K_2O: 0.40 Na_2O : 1 Al_2O_3 : 2.0 ± 0.1SiO_2 : x H_2O	3	NH_3 and H_2O from a N_2/H_2 flow
4A	1 Na_2O: 1 Al_2O_3: 2.0 ± 0.1 SiO_2 : x H_2O	4	H_2O, SO_2, CO_2, H_2S, C_2H_4, C_2H_6, and C_3H_6
5A	0.80 CaO : 0.20 Na_2O : 1 Al_2O_3: 2.0 ± 0.1 SiO_2: x H_2O	5	H_2S, CO_2 and mercaptans removal from natural gas
13X	0.80 CaO : 0.20 Na_2O : 1 Al_2O_3: 2.0 ± 0.1 SiO_2: x H_2O	N/A	H_2O, CO_2, H_2S, mercaptan removal from hydrocarbon/natural gas

Composite Sorbents

The current approach is to combine the advantages of liquid solvent, membrane process and adsorption for regenerable CO_2 removal sorbents for low concentration applications such as in Alkaline Fuel Cells (AFCs), Metal-Air batteries, and portable life

support systems by adapting the Banefield process. The Banefield process uses hot K_2CO_3(aq) to react with CO_2 in the presence of moisture as follows:

$$H_2O + CO_2 \Leftrightarrow H_2CO_3$$

$$H_2CO_3 \Leftrightarrow H^+ + HCO_3^- \qquad K_a = 4.3\text{x}10^{-7}$$

$$HCO_3^- \Leftrightarrow H^+ + CO_3^{2-} \qquad K_a = 5.6\text{x}10^{-11}$$

$$2H^+ + CO_3^{2-} + K_2CO_3 \Leftrightarrow 2KHCO_3$$

$$K_2CO_3 + CO_2 + H_2O \Leftrightarrow 2KHCO_3 \qquad (1)$$

The reaction is initiated by diffusion of carbon dioxide from the gas phase to the water layer on the surface. This water layer can be formed by water adsorption or excess water provided during sorbent preparation. Carbonic acid, a product from carbon dioxide dissolved in water, is a weak acid and dissociated in two steps and then neutralized by K_2CO_3 forming $KHCO_3$.

Many commercial processes for CO_2 removal employ the Banefield process. However, the use of liquid solvents is difficult in practice especially to downsize the unit. Thus, the development of a new material for a cost-effective filtration with high CO_2 adsorption capacity and ability to regenerate is needed. The current approach is to utilize the liquid potassium carbonate in packed bed operations for CO_2 removal under the moist conditions. The porous microfibrous media [20-22] is used to entrap K_2CO_3(aq) as an "apparent solid" by incipient wetness impregnation. The use of small particulates significantly enhances the intraparticle diffusion and allows high contacting efficiency.

The nano-dispersed nature of K_2CO_3 combined with the use of small support particulates promotes high K_2CO_3 utilization, high contacting efficiency, and high accessibility of K_2CO_3 while minimizing the pressure drop and lowering the heat of reaction generated as shown in Table 7.

Table 7: Adiabatic heat of selected CO_2 sorbents

Sorbents	Chemical Reaction	δH (kJ/mol) @25°C	δT (K)
LiOH	$2LiOH + CO_2 \Leftrightarrow Li_2CO_3 + H_2O$	-88.53	120
CaO	$CaO + CO_2 \Leftrightarrow CaCO_3$	-178.33	259
$Ba(OH)_2$	$Ba(OH)_2 + CO_2 \Leftrightarrow BaCO_3 + H_2O$	-162.31	218
	$K_2CO_3 + CO_2 + H_2O \Leftrightarrow 2KHCO_3$	-100.20	120
K_2CO_3	$K_2CO_3 + CO_2 + H_2O + ACP \Leftrightarrow 2KHCO_3 + ACP$	-100.20	15

A high heat generation of sorbents is a drawback since it will require a cooling system meaning high energy consumption and capital cost. Based on the data in Table 7, LiOH system has a fairly low heat of reaction compared to CaO and $Ba(OH)_2$; however, the system is not regenerable. An alternative, K_2CO_3 system with the same adiabatic temperature rise, the K_2CO_3 system has a slightly higher heat of reaction than LiOH. However, the K_2CO_3 system can be regenerated. By utilizing incipient wetness impregnation, K_2CO_3 can be entrapped in the porous support matrix, e.g. activated carbon particulates (ACP). The high dispersion nature of the support materials will allow the reduction in adiabatic temperature rise.

Methods for Sorbent Preparation

It is known that the preparation procedures affect sorbent characteristics, such as compositions, crystal structure, and homogeneity of the sorbents. By tailoring the preparation procedure, the desire characteristics of the sorbents can be controlled. There are two main methods for sorbent preparation: precipitation and incipient wetness impregnation.

Precipitation

This method involves the use of two or more chemically reactive chemical compounds in the aqueous solutions or suspension to form precipitation. The general rule of thumb is that the chemical reagents have to have high solubility in water. These precipitates can present in the form of single metallic compounds, alloys, metal hydroxide, or metal carbonate depending on the reactions between the metal salts. They can be converted into metal oxides by calcination in a presence of oxygen (air) or in a reducing atmosphere (i.e. He) to reduce the metal oxide to metal. This method is suitable for sorbent preparation in bulk; however, it is difficult to control the composition and the amount of the sorbent formed due to the possibility of side reactions.

Impregnation

Impregnation is another way of forming a composite sorbents by utilizing the porous support materials. The sorbents are prepared by dissolving a metallic compounds, which then come into contact with the support materials. The impregnated materials are then calcined or dried at selected temperature and atmosphere to control the formation of the

compound. The choice of the support materials and calcination temperature is one of the most important factors for a desire composite sorbent formation. Zhang et al [23] studied the metal oxide-support interaction of Li_2O and γ-Al_2O_3. The result suggested that Li_2O diffuses into the bulk γ-Al_2O_3 forming α-$LiAlO_2$ at 733-793K. Incipient wetness impregnation method allows the control over the amount of the active materials added and the sorbents usually are generated in the porous structure of the support materials.

Adsorption

Adsorption is a process that materials at the interface between two phases accumulate. These phases can be any combination of liquid, solid, and gas. The adsorbing phase is called adsorbent and the materials being adsorbed are called adsorbate.

Adsorption is the result of interactive forces of an attraction at the surface between porous solids and adsorbate molecules removed from the fluid surrounding the solids. This interactive force at the surface consists of permanent dipole, induced dipole, quadrupole electrostatic effects known as van der Waal's forces. Physical adsorption is a phenomenon due to van der Waal's forces, or the forces of attraction between non-polar molecules. Electrostatic forces, or forces due to charged species, also play an important role in physical adsorption especially when the adsorbent is a charged species such as a zeolite. Physical adsorption is always an exothermic process and the heat of adsorption provides a direct measure of the strength of the bond between adsorbate and adsorbent.

Physical adsorption is separate from chemical adsorption or chemisorption, where a chemical bond is formed and electrons shared between the adsorbent and adsorbate. Physical adsorption is considered a weak force and normally characterized by forces between molecules less than R*T, where R is the universal gas constant and T is the absolute temperature. Chemisorption involves stronger forces with energies normally larger than R*T. At room temperature R*T is about 2.5 kJ/mol.

Adsorption on the solid adsorbents has great potential for environmental applications as the process can effectively remove pollutants from both liquid or gas environments, which allows many possibilities for a wide range of applications, such as CO, CO_2, and H_2S. Due to the high degree of purification, adsorption on solid sorbents is usually used at the end of the treatment sequence as a packed bed.

Adsorption should not be confused with absorption, as they are two very different phenomena. Adsorption is the accumulation of concentration on the surface of a solid; absorption is the accumulation of concentration within the bulk of a solid or liquid.

The most common means of gas-phase adsorption is by passing contaminated gas through an immobilized bed of particulates, also known as a packed bed or fixed bed adsorber. In a packed bed, adsorption occurs in the mass transfer zone (MTZ). This is the zone where adsorbate molecules from the feed are transferred to the solid adsorbent. As the adsorbent particles in this zone become saturated, the zone moves slowly through the bed in the direction of gas flow. Breakthrough occurs when the zone reaches the exit of the bed. Areas upstream and downstream of the MTZ are not involved in the adsorption process. Upstream of the MTZ, adsorbent particles are saturated and in equilibrium with the gas carrying the contaminant through the bed. Downstream of the

MTZ, no challenge is present in the gas passing through the bed and thus no adsorption is occurring.

Microfibrous Media (MM)

Microfibrous media (MM) have great potential to enhance mass and heat transfer of the adsorption and catalytic processes compared to the use of the packed beds of particulates [24,25]. For conventional adsorption process using porous adsorbents, the rate of adsorption depends on two major factors: interparticle diffusion and intraparticle diffusion. Interparticle resistance is the mass transport resistance between the flowing gas and the adsorbent particle, also called the film resistance. This resistance is often considered as a constant and modeled as a stagnant film around the particle. Intraparticle resistance is the mass transport resistance inside the adsorbent particle and is a function of the pore type and pore structure [26]. As a result, most adsorption processes are intraparticle-limited mass transport. A decrease in particle size increases the proportion of interior surface area to exterior surface area and results in an increase in the overall adsorption rate. Adsorption will take place faster and allow more adsorbents to be utilized. However, small particle size leads to high pressure drops in packed bed adsorbers as seen in the Ergun equation:

$$\frac{\Delta P}{L} = 150\frac{\mu v_o}{\varepsilon^3}\left(\frac{1-\varepsilon}{D_p}\right)^2 + 1.75\frac{\rho v_o^2}{\varepsilon^3}\frac{(1-\varepsilon)}{D_p}$$

where ΔP is total pressure drop, L is bed depth or length, μ is viscosity, v_o is the linear gas velocity through the bed, ε is the void fraction of the bed (commonly 0.6), D_p is particle diameter, and ρ is gas density.

In industrial adsorption processes, the use of small adsorbents results in high adsorption efficiency, but it is not practical due to high pressure drop or high energy consumption. The current effort is to utilize small particulates to reduce the intraparticle-limited mass transport and still maintain the high adsorption efficiency by means of microfibrous media.

Composite Bed

A large packed bed usually has a high capacity due to high volume loading of sorbent. However a packed bed of large particulates makes poor use of the sorbent as evidenced by a slow, sigmoidal breakthrough curve as shown in Figure 6. A decrease in the size of the particle increases the breakthrough time of the packed bed [27], but at the same time the pressure drop through the packed bed also increases. It is evident that the particle size affects the pressure drop through the bed and the rate of diffusion into the particles. As a result, most commercial packed bed adsorbers sacrifice high adsorption capacity to maintain low pressure drop. The concept of composite beds is then introduced. A composite bed refers to the combination of a standard packed bed with a thin layer of MM at the outlet. MM acts as a polisher removing small amounts of challenge as they break through the packed bed. The polishing layer in a composite bed has high contacting efficiency from the small entrapped particles in the MM. The breakthrough curve of the MM layer alone is very sharp indicative of high sorbent utilization, but breakthrough times are low as expected due to a low volume loading of the sorbent. The synergistic effect of the composite bed is much greater than the simple addition of the breakthrough times of each layer. Low outlet concentrations exiting the packed bed are

introduced into the high contacting efficiency polishing layer. The first bed adsorbs a large percentage of the inlet challenge, so the MM layer only needs to polish or adsorb the remainder.

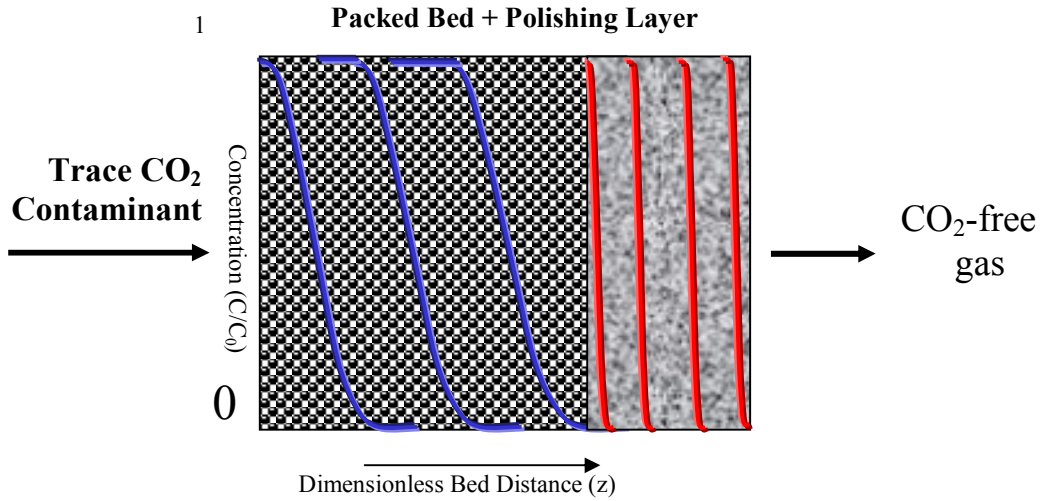

Figure 6: Concentration Profiles in a Composite Bed

This composite bed can be described by a bed depth service time equation (BDST) [28], which is usually used for packed bed of particles with a strong physical adsorption. The BDST equation is often used to determine the required time in the bed for a given challenge concentration to be adsorbed.

$$t = \frac{N_o}{C_o v_o}\left(L - \frac{v_o}{kN_o}\ln\left(\frac{C_o}{C_b} - 1\right)\right)$$

Where t is time required for adsorption, v_o is linear gas velocity through the bed (also known as face velocity), L is adsorbent bed depth, k is the overall adsorption rate

constant, N_o is the mass per unit volume of adsorbent, C_o is influent concentration, and C_b is concentration at breakthrough. A thicker bed for higher adsorption effectiveness is balanced with the fact that pressure drop increases linearly with bed thickness as evident in the Ergun equation.

Cahela and Tatarchuk [29] adapted this bed depth service time equation to describe the composite bed of microfibrous media incorporation. If the amount of challenge removed until breakthrough by the MM layer alone (concentration*time area) is converted to an equal area underneath the packed bed breakthrough curve, a good estimate of the composite bed breakthrough time is obtained as shown in Figure 7. This is known as the Equal Areas Design Rule.

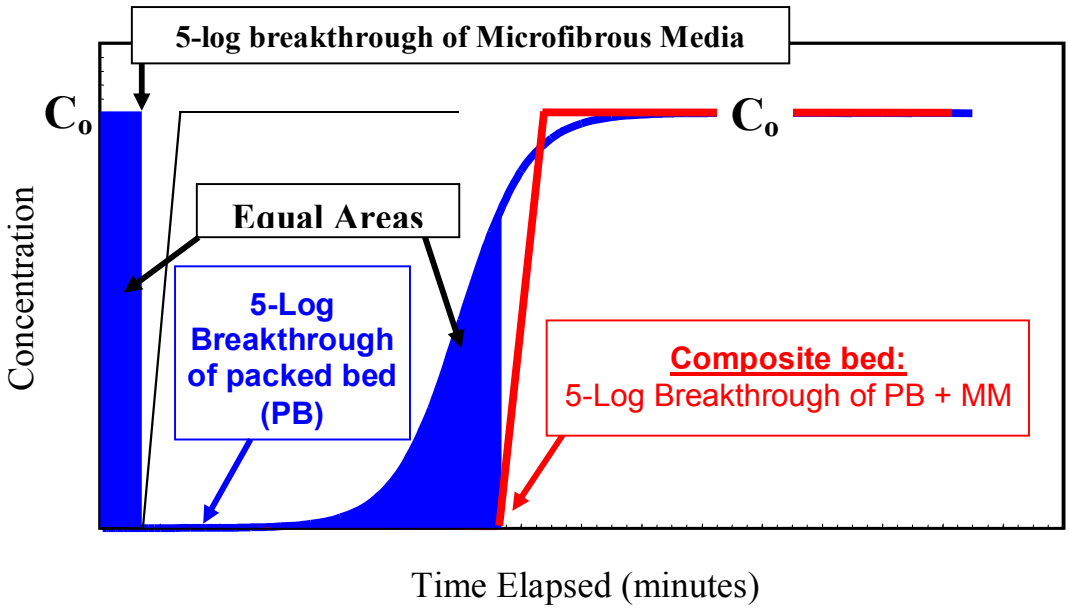

Figure 7: Equal Area Design Rule

Modeling Adsorption Breakthrough

Adsorption systems for gas or liquid purification usually employ a packed bed adsorber. To design adsorbers effectively, the dynamics and characteristics of the systems are required. The three main parameters are the adsorption isotherm, the external mass transfer coefficient, and the intraparticle mass transfer coefficient. Many theoretical models have been developed for modeling adsorption breakthrough curves, such as the effective diffusion model, the combined diffusion model under the assumptions of: (1) negligible pressure drop, (2) constant hydraulic loading, (3) negligible dispersion, (4) isothermal conditions, and (5) constant surface diffusion coefficient.

Yoon and Nelson [30] have developed a model describing adsorption breakthrough curves on activated charcoal based on assumption that the rate of adsorption decreases as a function of adsorbate adsorption. This equation is simple and required no data on characteristics of the adsorbates and adsorbents. As a result, this model will be applied throughout this study. The Yoon and Nelson equation can be expressed as follows:

$$t = \tau + \frac{1}{k'} \ln \frac{C_b}{C_i - C_b}$$

where k' is the rate constant (1/min), τ is the time required for 3% adsorbate breakthrough(min), t is the (sampling) breakthrough time (min), C_b is the breakthrough (effluent) concentration of adsorbate (ppm), C_i is the initial inlet concentration of adsorbate (ppm).

These values are determined from the experimental data by plotting $\ln[C_b/(C_i-C_b)]$ vs. time (t) according to Yoon and Nelson equation. If the accurate experimental data are obtained, this plot will result in a straight line with a slope of k' and the intercept of $-k'\tau$.

Critical Bed Depth

Critical bed depth (CBD), or theoretical minimum bed thickness required for adsorption of a given challenge. Critical bed depth is obtained from the bed depth service time equation by setting t = 0 and solving for L:

$$CBD = \frac{v_o}{kN_o}\ln\left(\frac{c_o}{c_b}-1\right)$$

If the thickness of a packed bed is less than critical bed depth, there will be an immediate breakthrough. Critical bed depth is useful in comparing different adsorber designs as it gives a measure of overall effectiveness.

Sorbent Utilization

Overall efficiency of an adsorbent bed can be evaluated by different parameters. In this study, sorbent utilization is used by the following definition:

$$Utilization = t_{BT}/t_{theo}$$

where t_{BT} is the time required for the 3% adsorbate breakthrough, t_{theo} is the time required for the 100% adsorbate known as saturation time.

II. EXPERIMENTAL

Many types of sorbents were tested in this study, such as Molecular sieves (3A, 4A, 5A, ad 13X), Baralime®, Carbolime®, Sodalime®, and K_2CO_3 impregnated onto various support materials.

Adsorbent Preparation

Supported K_2CO_3 sorbents were prepared using K_2CO_3*1.5H_2O as a precursor, which is loaded onto the support by pseudo-incipient wetness impregnation. Three types of support materials were selected based on their liquid holding capacity (pore volume): Al_2O_3, SiO_2, and activated carbon. The characteristics of these support materials are shown in Table 8.

Table 8: Physical properties of porous host matrix

Host Matrix	Density (g/cc.)	Pore Volume (cc./g)	Manufacturer
ACP	0.48	0.60	PICA USA
SiO_2	0.512	0.60-0.70	Selecto Scientific, Inc.
Al_2O_3	0.387	1.14	Alfa Aesar

The sorbents were then prepared by filling the pores of the porous supports at various loadings by varying the solution concentration to examine the effect of K_2CO_3 loading on CO_2 adsorption performance. The impregnation solution was prepared by adding potassium carbonate sesquihydrate and dionized water to obtain a desire concentration. After impregnation, the sorbents were then dried at 100^{o}C for 30 minutes. The volume of the sorbents was maintained at 10 cc; otherwise stated. The influence of the nature of host matrix on the adsorption capacity was studied.

Microfibers

Three types of microfibers can be used: Polymer fibers, nickel fibers, and glass fibers. Physical properties of microfibers are shown in Table 9.

Table 9: Physical properties of microfibers

Factors\Fiber type	Metal	Ceramic	Polymer
Volume Loading	3%	4%	4%
Fiber Density	8 g/cc	2.4 g/cc	1 g/cc
Fiber Diameter	2-12 μm	<1-12 μm	10-20 μm
Operating Temperature	150-600 ^{o}C	600-900 ^{o}C	<150 ^{o}C
Cost	$60/lb	$7/lb	$1/lb

Different microfibers are used mainly based on the type of operating temperature ranges. Polymer fibers, for example, are light and cheap. As a result, they are often used in air-purifying respirators to scrub trace contaminants, such as H_2S and CO. Due to their sensitivity to temperature (<150^{o}C), the use of polymer fibers often limits to disposable filters or regeneration has to be done through PSA to maintain the robust structure of the polymer microfibrous media. For Metal fibers, the operating temperature is between 150-600^{o}C, which allows this type of fibers to be used in combination with adsorbents or catalysts of high exothermic reactions [31,32]. Even though the use of nickel fibers allows higher operational temperature ranges, it should be noted that nickel fibers can get oxidized in the presence of H_2O and/or O_2. As a result, the microfibrous media formed from nickel

fibers tend to gradually corrode over adsorption/regeneration in the presence of H_2O and O_2. The glass fibers offer the operational temperatures (900^oC), which allows this type of fibers to be used in a wide range of applications [33]. The nickel microfibers were selected in this study due to operating temperature of the adsorption tests and the range of regeneration temperatures as well as the high thermal conductivity of the nickel fibers that allows the reduction in thermal effects.

Preparation of Microfibrous Entrapped Sorbents

A sintered metal microfibrous carrier was used to entrap 150-250 μm diameter support particulates by wet layer paper-making/sintering procedure. The composition of 8" preform media is shown in Table 10.

Table 10: Composition of 8" Preform

Component	**Weight (g)**
8 μm nickel fibers	1
12 μm nickel fibers	3
Cellulose	1
150-250 μm particulates	10

1g of 8 μm nickel fibers, 3 g of 12 μm nickel fibers, and 1 g of cellulose were added into water and stirred vigorously to produce a uniform suspension. The produced suspension and 10 g of 150-250 mm ACP were mixed in an 8" perform former under aeration. 8" perform was then formed by vacuum filtration followed by drying in a heat drum. The preform is then sintered in hydrogen atmosphere at 900^{o}C for two hours to get rid off the cellulose in the preform and nickel fibers to come into contact and form a sinter-locked matrix. By utilizing the wet layer papermaking process, these particulates can be entrapped uniformly in the fibrous matrix as shown in the SEM micrograph in Figure 8.

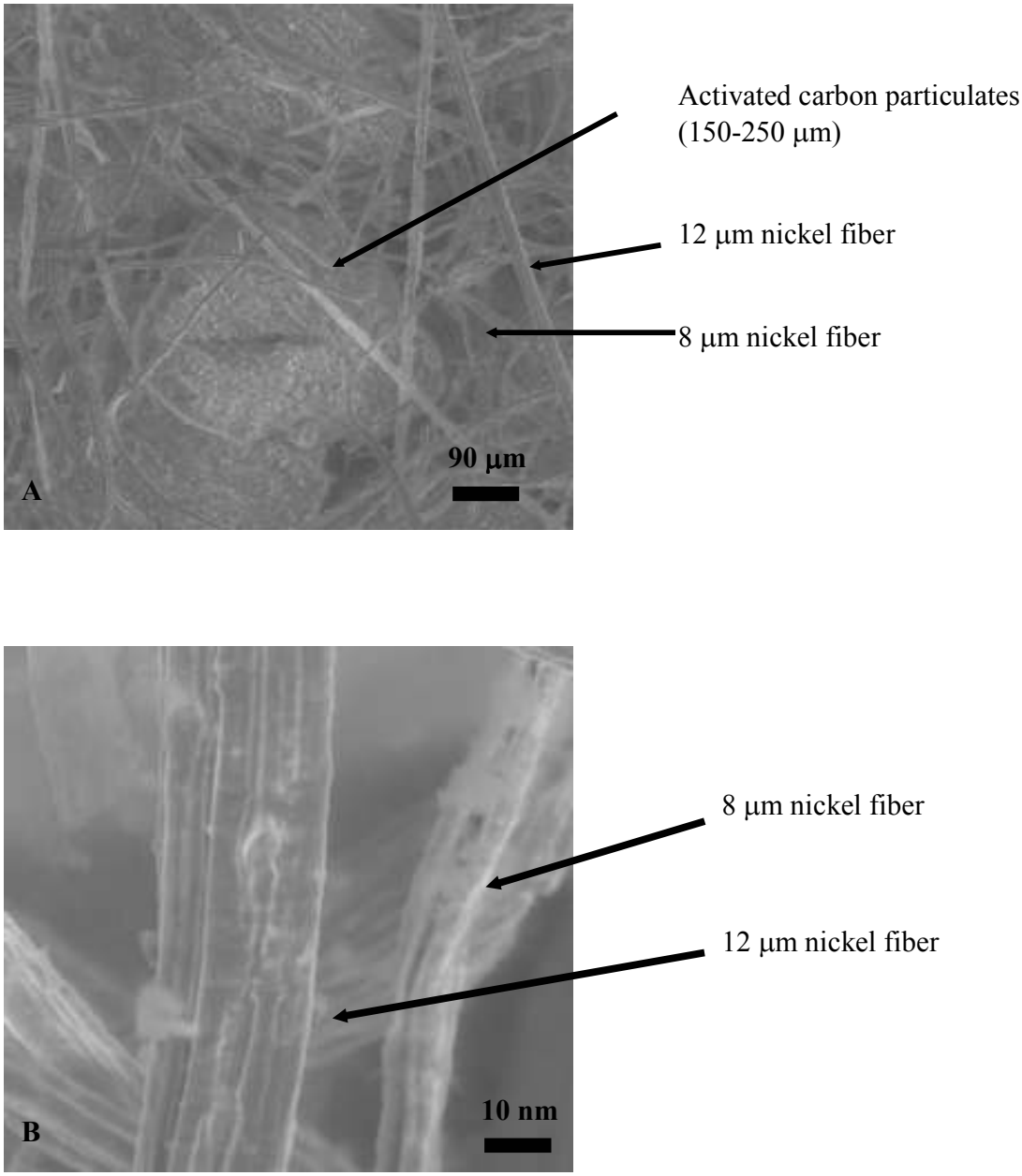

Figure 8: SEM micrographs of Microfibrous Media

A: Microfibrous entrapped ACP
B: Microfibrous Matrix

Figure 8B shows 12 μm and 8 μm nickel fibers. Figure 8A shows a microfibrous media consisting of 12 μm and 8 μm nickel fibers forming a 3-D sinter-locked matrix structure to entrap activated carbon particles of 150-250 μm.

Breakthrough Tests

The performance of adsorptive materials used for carbon dioxide removal was studied at 20-30^{o}C in a packed-bed adsorber (1.5 cm ID) using simulated gas containing 1.5 vol.% CO_2 (C_0). The gas flux was then saturated with water vapor up to 2 vol.% (84% RH) prior to entering the reactor inlet at room temperature as shown in Figure 9.

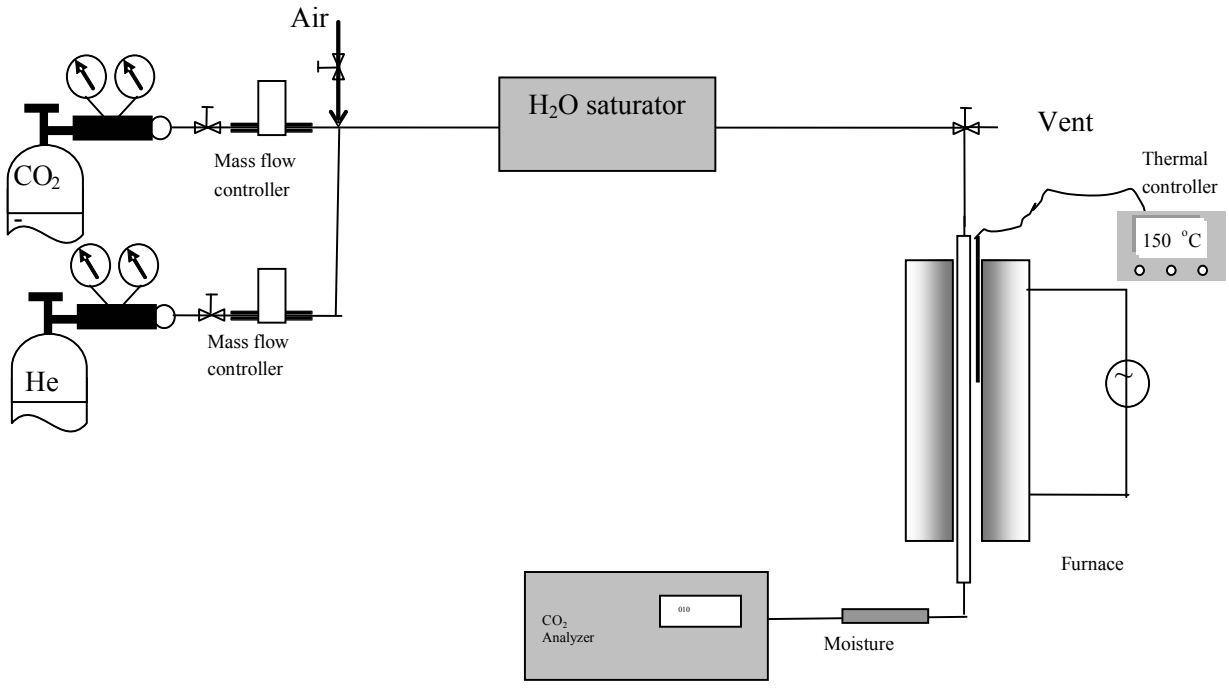

Figure 9: Experimental apparatus

The outlet CO_2 concentration was determined by CO_2 analyzer (PP Systems, USA) shown in Figure 10.

Figure 10: Non-dispersive Infrared CO_2 Analyzer

The CO_2 analyzer was calibrated against air and can detect CO_2 concentration as low as 1 ppm by utilizing Non-dispersive infra-red gas analysis to detect CO_2. The downstream concentration (C) was recorded simultaneously at the sampling rate of 1 data point per second. The test results are expressed in term of variations of C/C_0 over time (breakthrough curves). The breakthrough concentration is defined at 50 ppm; otherwise stated.

Sorbent Characterization

The structural phase composition of the sorbents was then characterized by X-ray diffraction (XRD) using CuKα radiation from 20° to 60° with the scanning rate of 4°/min. Figure 11 shows XRD patterns of K_2CO_3*1.5H_2O, K_2CO_3, and $KHCO_3$, all of which are used as references for phase identification.

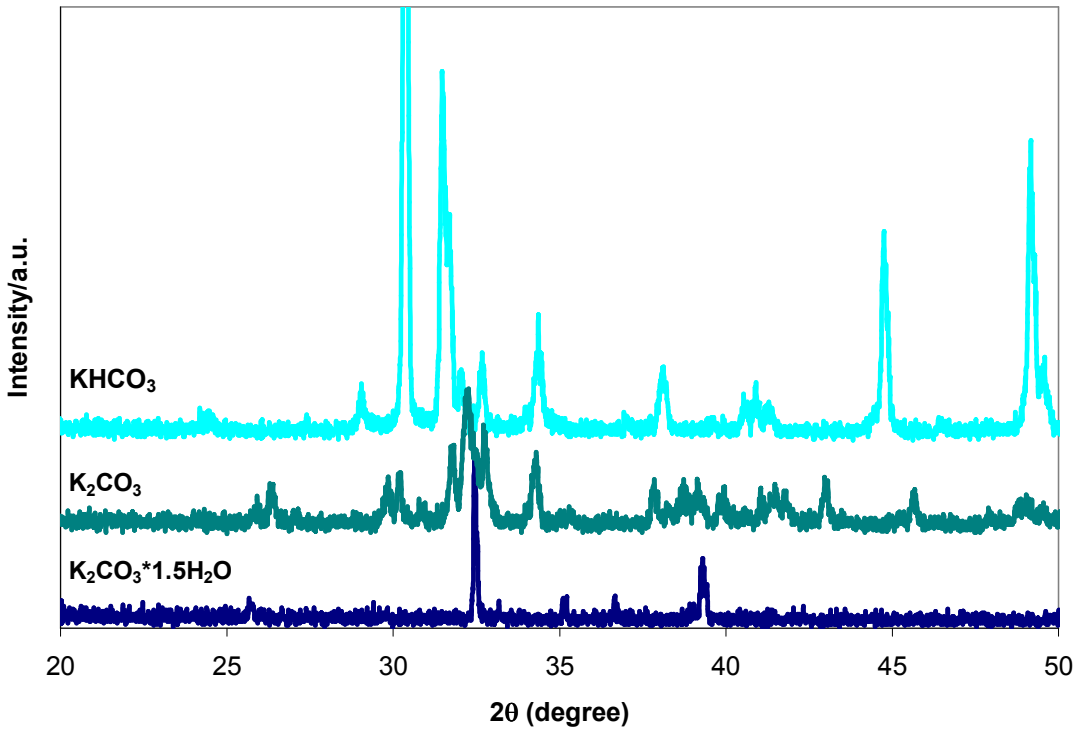

Figure 11: XRD patterns of K_2CO_3*1.5H_2O, K_2CO_3, and $KHCO_3$

Differential Scanning Calorimetry (DSC) was then used to determine the thermal stability of the sorbents at temperatures between 35 and 500°C at the heating rate of 10°C/min to determine the regeneration temperature. Scanning Electron Microscopy (SEM) was then

employed to examine the robustness and structural integrity of the microfibrous media after cyclic adsorption/desorption.

Composite Bed

The composite bed consists of a packed bed of sorbent particulates followed by a polishing sorbent layer as shown in Figure 12. The influence of microfibrous media incorporating adsorption of solid sorbents on the breakthrough characteristics was studied.

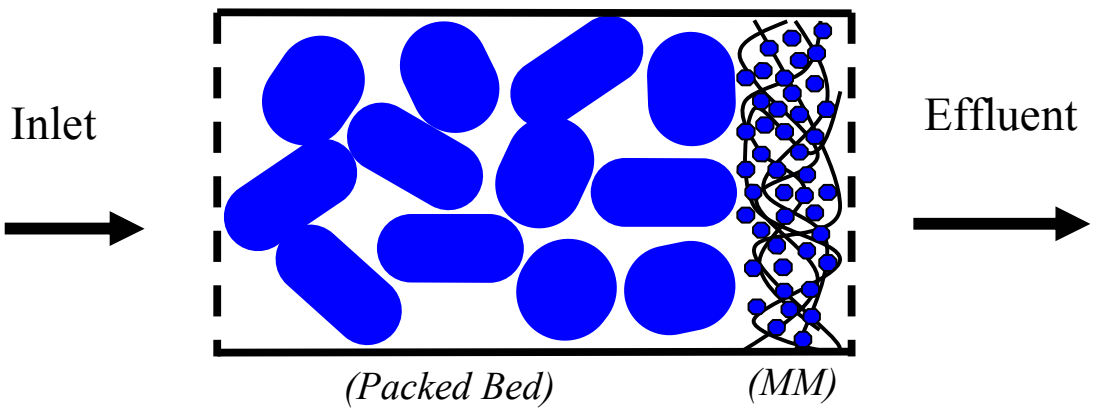

Figure 12: Composite Bed Design

A series of supported-K_2CO_3 sorbents were prepared in order to examine and compare the performance of a packed bed of K_2CO_3/ACP sorbents, composite, and the packed bed of K_2CO_3/ACP with the same volume as the composite bed. A packed bed of Sodalime was then applied in a composite bed utilizing microfibrous media entrapped K_2CO_3/ACP

sorbents as a polisher and performed breakthrough tests against the packed bed of Sodalime of the same volume for comparison.

IV. PRELIMINARY BREAKTHROUGH TESTS OF SELECTED SORBENTS

Selected solid sorbents, such as molecular sieves 3A, 4A, 5A, 13X, Sofnolime, Baralime, and Carbolime undergo breakthrough tests to measure their carbon dioxide adsorption capacity. The basic properties of these sorbents are shown in Table 11.

Table 11: Characteristics of Selected Adsorbents

Adsorbent	Particle Size	Density	Manufacturer
3A	1.6 mm	0.6550 g/cc.	Alfa Aesar
4A	1.6 mm	0.7045 g/cc	Alfa Aesar
5A	1.6 mm	0.6685 g/cc.	Alfa Aesar
13X	1.6 mm	0.5963 g/cc.	Alfa Aesar
Sofnolime	1.0-2.5 mm	0.8715 g/cc.	Molecular Product (UK)
Baralime	2.3-4.7 mm	0.9207 g/cc.	Allied Healthcare Products
Carbolime	2.5-5.0 mm	0.7805 g/cc.	Allied Healthcare Products

The breakthrough tests were conducted by loading five grams of each sorbent in a packed bed adsorber (1.5 cm. ID) using 1.5% CO_2 challenge gas as a test gas. The breakthrough results are shown in Figure 13.

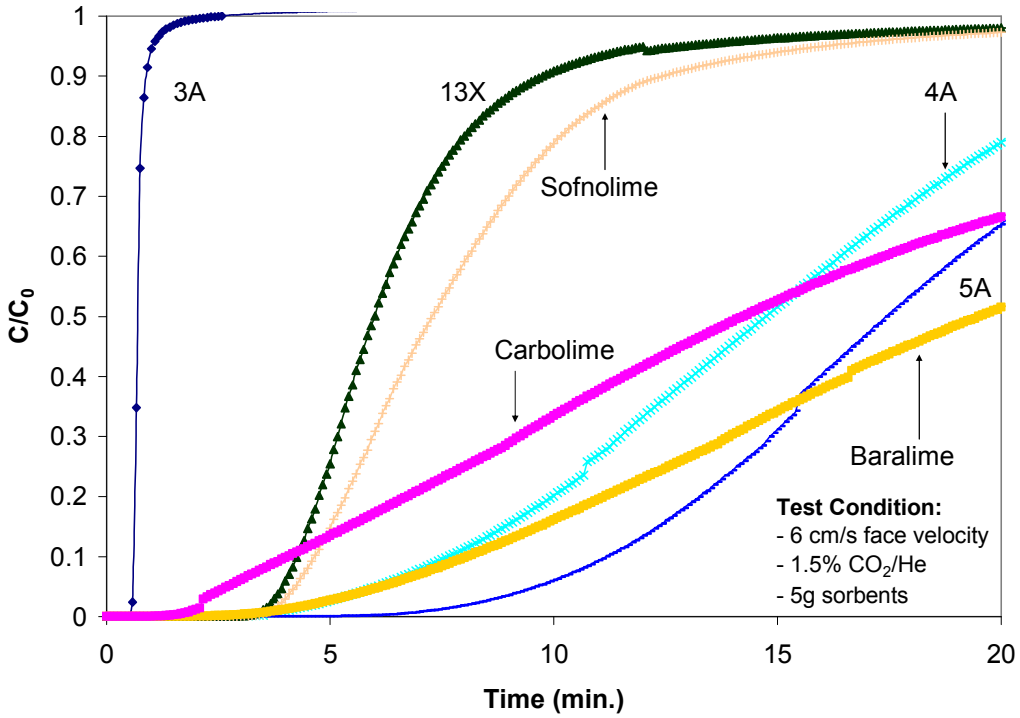

Figure 13: Breakthrough curves of selected adsorbents

The breakthrough curves obtained in Figure 13 show a various shapes of breakthrough curves indicating differences in adsorption mechanisms of sorbents. Among molecular sieves, 3A and 13X offer sharp breakthrough curves indicating high sorbent utilization. In the case of Sodalime, Sofnolime offers a sharp breakthrough curve compared to those of Carbolime and Baralime indicative a higher sorbent utilization. The carbon dioxide adsorption capacity was then calculated and tabulated as shown in Table 12.

Table 12: Breakthrough Data of Selected Adsorbents

	Weight	Volume	BT time	Saturation Capacity		Utilization
	g	cc.	min	g CO_2/g sorbent	g CO_2/cc.	%
3A	5.008	7.519	0.00	0.0000	0.0000	N/A
4A	5.009	7.097	3.04	0.0538	0.0379	24
5A	5.009	7.479	5.75	0.0660	0.0441	36
13X	5.009	8.385	2.75	0.0245	0.0146	54
Sofnolime	5.006	5.737	2.92	0.0296	0.0258	47
Baralime	5.011	5.431	2.50	0.0830	0.0764	15
Carbolime	5.003	6.406	1.08	0.0650	0.0507	11

Molecular Sieves (MS)

It is shown that molecular sieves exhibit CO_2 adsorption capacity in the sequence: 5A>4A>13X>3A. The use of MS utilizes the idea of physical adsorption of gas molecules with critical diameter less than the effective pore size of the MS. The number usually indicates the average pore size of the MS. In the case of carbon dioxide, CO_2 molecules have an average critical diameter of 2.8A. As a result, the MS with the effective pore size larger than 2.8A have potential to adsorb such species.

The use of molecular sieves for carbon dioxide removal in commercial applications is normally incorporated with other drying agents such as silica and 13X-MS. This is due to the competitive adsorption between CO_2-MS and H_2O-MS. NASA used two canister molecular sieves containing 5A for carbon dioxide removal and 13X for water removal during SKYLAB. The desorbed carbon dioxide was vacuumed to space. Figure 14 shows breakthrough curves of molecular sieves 5A in dry gas and wet gas of 1.5%CO_2.

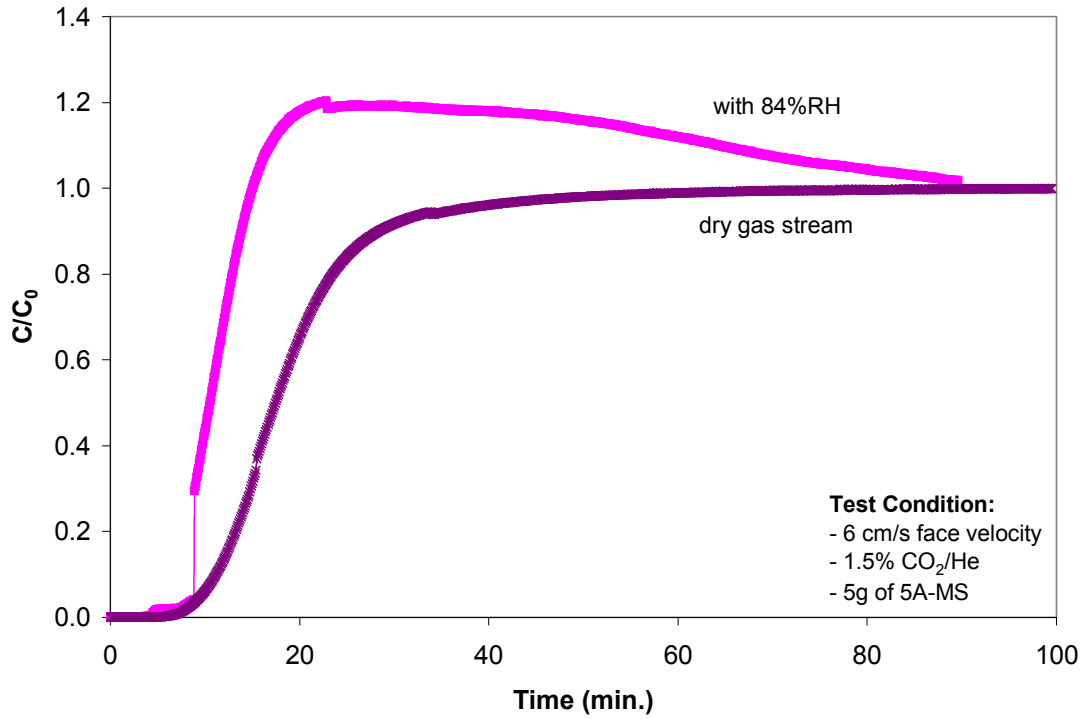

Figure 14: Breakthrough curves of Molecular Sieves 5A in wet and dry gas

It is shown that additional water caused a decrease in CO_2 adsorption capacity as shown in the breakthrough curves. However, the breakthrough curve of additional water in the gas stream shows an increase in outlet concentration over the initial concentration ($C/C_0>1$) indicating carbon dioxide enrichment. In the presence of water, a competitive adsorption on the MS-5A between H_2O and CO_2 take place. However, molecular sieves adsorb water preferentially. As a result, once the packed bed of MS-5A is fully saturated; MS-5A is then released carbon dioxide in order to accommodate water as shown in an overshoot of the carbon dioxide.

Sodalime

Sodalime is usually used for carbon dioxide removal processes from a close-circuit breathing systems by utilizing chemical reaction on the solid sorbents based on hydroxides of alkali metals. The major component of these sorbents is calcium hydroxide activated with sodium hydroxide or potassium hydroxide as shown in the following reactions:

$2NaOH + CO_2 \rightarrow Na_2CO_3 + H_2O$

$KOH + CO_2 \rightarrow K_2CO_3 + H_2O$

$Ca(OH)_2 + CO_2 \rightarrow CaCO_3 + H_2O$

There are many types of Sodalime depending on the hydroxide of alkali metal components, most of which are often used in military applications, such as in submarines and diving apparatus as well as in medical and chemical applications to purify anesthetic and industrial gases. The breakthrough data in Figure 13 show that carbon dioxide adsorption capacity in a sequence: Baralime>Carbolime> Sofnolime.

Baralime is another type of sorbents with barium hydroxide as an additive to increase the adsorption rate. Baralime consists of $Ba(OH)_2*8H_2O$ and $Ca(OH)_2$ and reacts with the carbon dioxide by the following reactions:

$Ba(OH)_2*8H_2O + CO_2 \rightarrow BaCO_3 + 9H_2O$

$H_2O + CO_2 \Leftrightarrow H_2CO_3$

$H_2CO_3 \Leftrightarrow H^+ + HCO_3^-$ $\qquad K_a = 4.3x10^{-7}$

$HCO_3^- \Leftrightarrow H^+ + CO_3^{2-}$ $\qquad K_a = 5.6x10^{-11}$

$2H^+ + CO_3^{2-} + Ca(OH)_2 \rightarrow CaCO_3 + 2H_2O$

$2H^+ + CO_3^{2-} + KOH \rightarrow K_2CO_3 + 2H_2O$

$K_2CO_3 + Ca(OH)_2 \rightarrow CaCO_3 + 2KOH$

Due to the crystallization water of barium hydroxide, the reaction between barium hydroxide can take place rapidly; however, calcium hydroxide has to form a water environment of dissolve in water surface for chemisorption with carbon dioxide to take place. Carbonic acid, a product of carbon dioxide dissolved in water is chemically bonded on the surface of the sorbents as a surface layer. As a result, the diffusion through the surface layer controls the rate of adsorption. The adsorption rate depends on the solubility of the main hydroxide of alkali metals ($Ca(OH)_2$). Selected solubilities of some hydroxide of alkali metals are shown in Table 13.

Table 13: Solubility of selected alkali metals

Hydroxide of alkali metal	Solubility in water (20^oC)
	g/100 g H2O
$Ba(OH)_2*8H_2O$	3.89
KOH	112
$Ca(OH)_2$	0.165
NaOH	109

For the sorbents consisting of sodium hydroxide, the chemical reactions are similar to those presented in the case of Baralime. The difference is on the activation reaction at the beginning of the reaction:

$$H_2O + CO_2 \Leftrightarrow H_2CO_3$$

$$H_2CO_3 \Leftrightarrow H^+ + HCO_3^-$$

$$HCO_3^- \Leftrightarrow H^+ + CO_3^{2-}$$

$$2H^+ + CO_3^{2-} + 2NaOH \rightarrow Na_2CO_3 + 2H_2O$$

$$Na_2CO_3 + Ca(OH)_2 \rightarrow CaCO_3 + 2NaOH$$

A better solubility of sodium hydroxide than calcium hydroxide is important for the chemisorption of carbon dioxide. Form the above reactions, water and sodium hydroxide have to be dissociated in order to yield high reaction efficiency by controlling the proper concentration of sodium hydroxide and water. As a result, some manufacturers add moisture (12-19%) in the sorbents to improve dissociation of sodium hydroxide and enhance the adsorption capacity. Figure 15 shows breakthrough curves of Sofnolime under wet and dry conditions. It is shown that in the presence of water, the dissociation of sodium hydroxide is enhanced and results in higher carbon dioxide adsorption capacity.

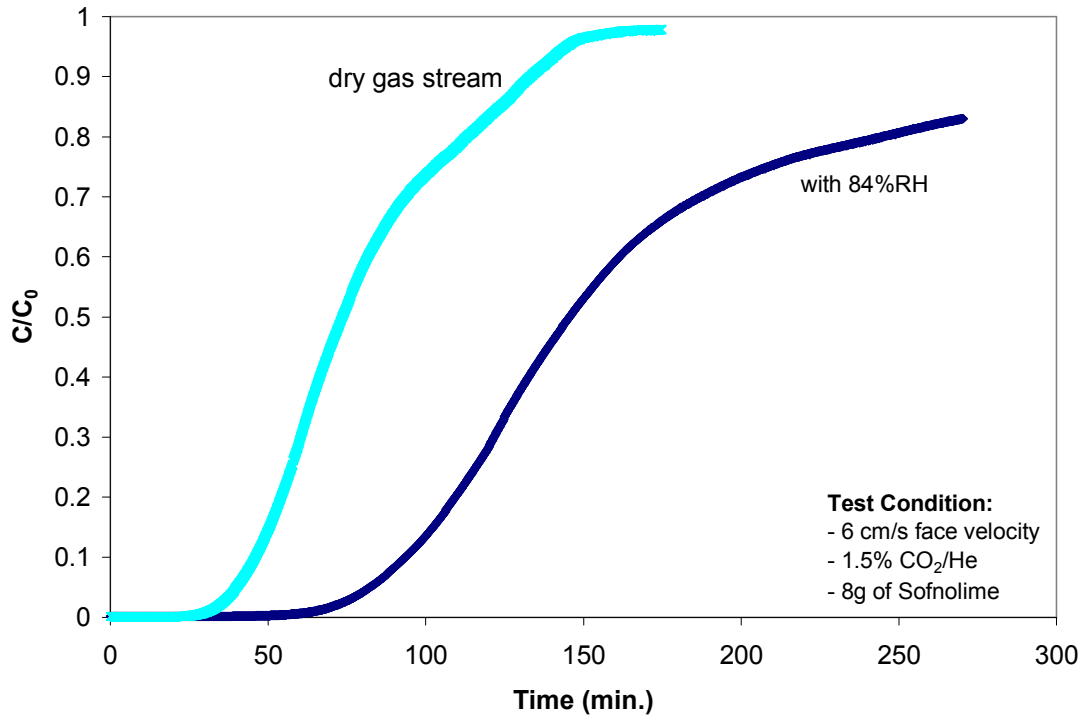

Figure 15: Breakthrough curves of Sofnolime in wet and dry gas

Summary:

Based on the data obtained from preliminary results, it is shown that molecular sieves 5A offers highest carbon dioxide adsorption capacity; however, for the use of molecular sieves, a guard bed is needed to remove moisture prior to removing carbon dioxide. In the case of Sodalime, water is rather necessary to create the water later on the surface of the sorbents and allows carbon dioxide adsorption reaction. As a result, many manufacturers add water to form crystallization water in the hydroxides of alkali metal to enhance the carbon dioxide adsorption capacity of the sorbents.

III. INFLUENCE OF POROUS HOST MATRIX

The development of the nano-dispersed chemically active compound into pores of the porous matrix reduces the internal mass transfer diffusion, improves utilization of the active compound, and lowers thermal effects (low regeneration temperature and δH of reactions). As a result, the composite sorbents were developed based on different types of porous support materials. The support materials were obtained from different manufacturers as shown in Chapter III. The support materials were then pulverized to obtain the size of 150-250 μm and 1 mm. The prepared composite sorbents consist of different amount of K_2CO_3 by varying the concentration of the impregnation solution. The composite sorbents were then drained the excess water prior to drying at 100^{o}C for 30 minutes. The carbon dioxide adsorption capacity tests were conducted at 20-30^{o}C in a packed bed adsorber of 60 cm length and 1.5 cm in diameter. The amount of the composite sorbent was maintained at 10 cc; otherwise stated. The adsorber was purged by He gas with the flow rate of 600 cc/min to remove the remaining of carbon dioxide in the adsorber. The breakthrough tests were conducted under wet gas (84 %RH) containing 1.5% CO_2. From the breakthrough curves, the CO_2 saturation capacity of the composite sorbents was then calculated as a ratio of the amount of CO_2 adsorbed by the sorbents and the amount of the sorbents loaded.

RESULTS AND DISCUSSION

K_2CO_3-on-SiO_2

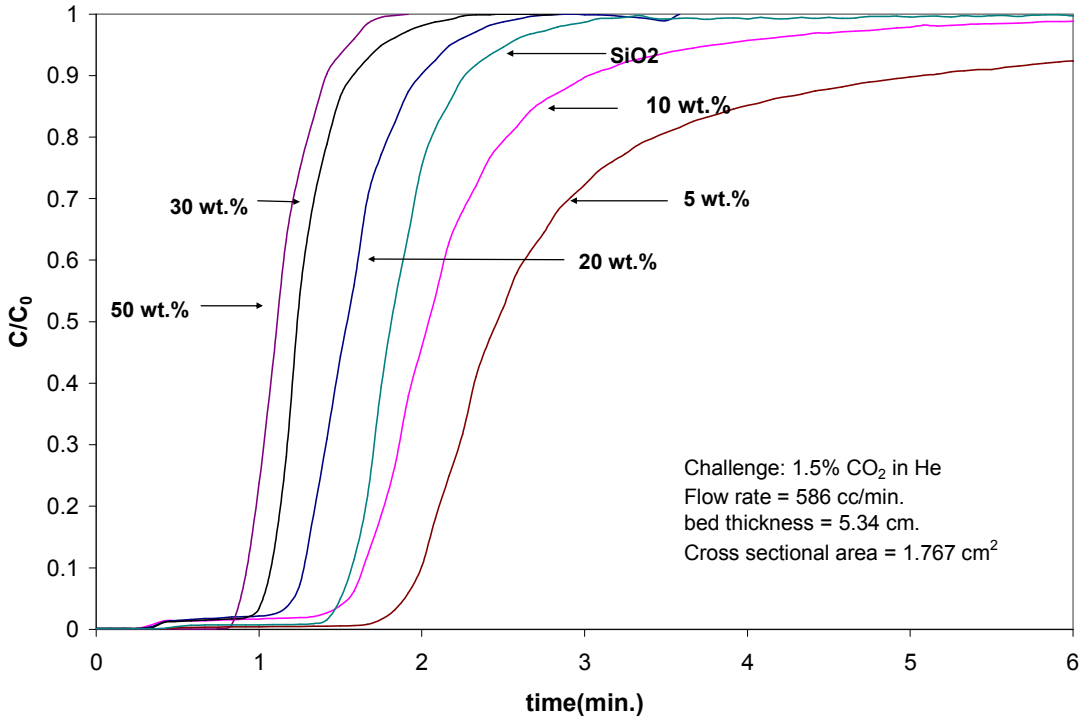

Figure 16: Breakthrough curves of K_2CO_3/ACP at different K_2CO_3 loadings

From the breakthrough curves shown in Figure 16, it is shown that the silica composite sorbents show sharp breakthrough curves indicative of high utilization of the composite sorbents, but low carbon dioxide adsorption capacity was observed on all samples. An increase in K_2CO_3 loading causes a decrease in carbon dioxide adsorption capacity as seen in the shift in breakthrough curves to the left side. It should be noted that there was an increase in volume after drying the prepared sorbents at 100^{o}C for 30 minutes. The carbon dioxide adsorption capacity as a function of K_2CO_3 loading was then calculated from the breakthrough curves as shown in Figure 17.

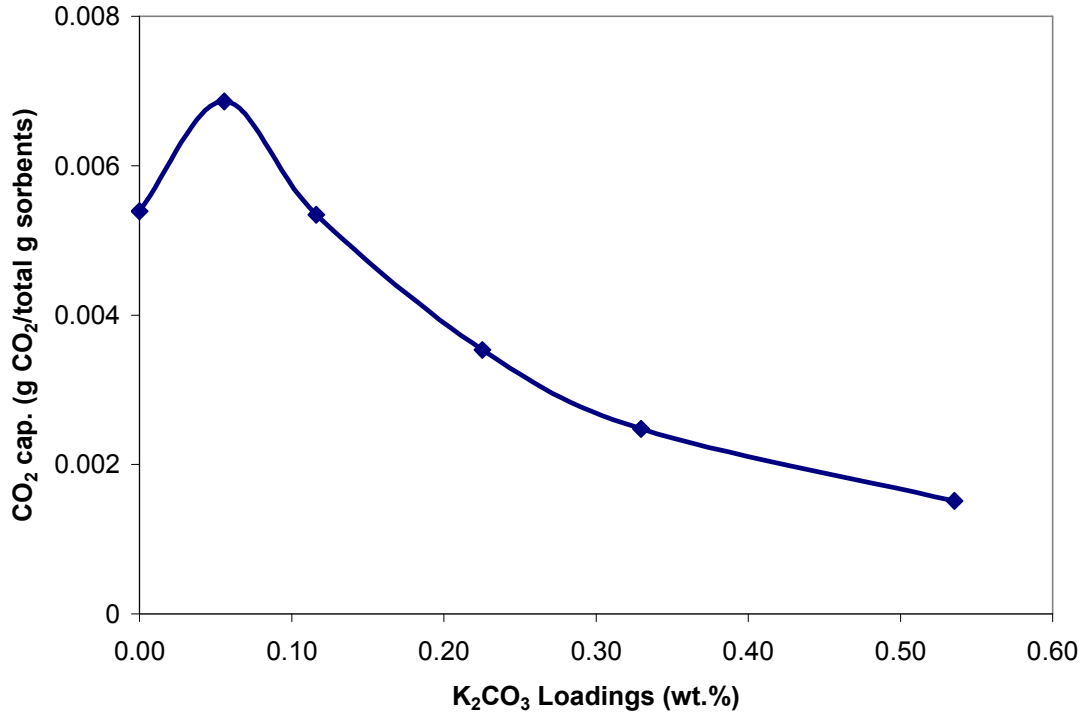

Figure 17: CO_2 adsorption capacity of SiO_2 composite sorbents as a function of K_2CO_3 loadings

Silica particles often used as a drying agent offer carbon dioxide adsorption capacity even though it is considerably low (residence time = 0.5 min) as shown in Figure 17. This might be due to the competitive adsorption between SiO_2-H_2O and SiO_2-CO_2. An increase in 5 wt.% K_2CO_3 loading shows a slight increase in carbon dioxide adsorption capacity, which does not exceed 0.0069 g CO_2/ total g of the composite sorbent. An increase in K_2CO_3 loaded onto silica from 5 wt.% to 10 wt.% caused a decrease in carbon dioxide adsorption capacity. A further increase in K_2CO_3 loading shows a further decrease in carbon dioxide adsorption capacity. The drop in capacity might be related to the chemical transformation during sorbent preparation between

potassium carbonate and silica forming an inactive phase on the surface of the composite sorbents. As a result, the silica composite sorbents were then analyzed by XRD to examine the chemical phase transformation.

XRD patterns in Figure 18 show the results of SiO_2 particles (for comparison) and K_2CO_3 impregnated SiO_2 with different K_2CO_3 loadings between 20 and 60 degrees. Silica particulates exhibit an amorphous structure with a broad peak indicating a presence of silica between 20 and 25°. An addition of K_2CO_3 onto silica particulates causes the surface reaction between SiO_2 and K_2CO_3 forming inactive K_2SiO_3 on the surface of SiO_2 as shown in the following reaction [34]:

$$K_2CO_3 + SiO_2 \Leftrightarrow K_2SiO_3 + CO_2$$

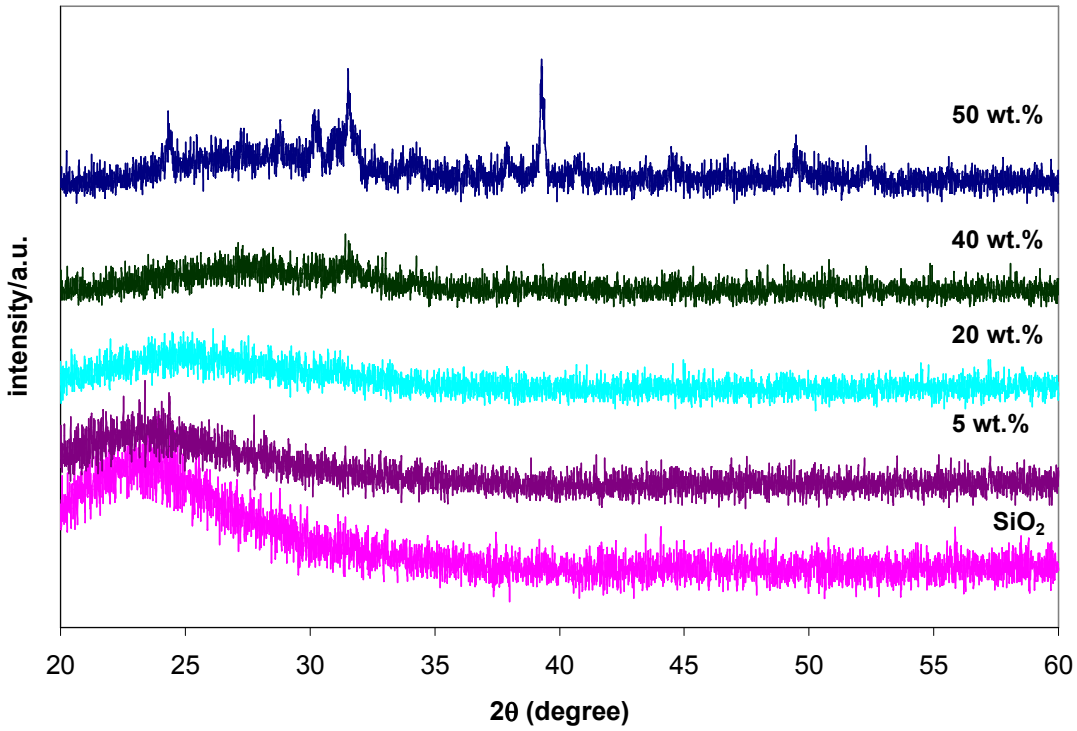

Figure 18: XRD patterns of SiO_2 and K_2CO_3 impregnated SiO_2

The formation of potassium silicate is shown in a decrease in silica peak (23^{o}); however no other phases were observed. Based on the breakthrough data and the XRD results, it is shown that silica alone can adsorb a low amount of carbon dioxide; however an increase in K_2CO_3 loading higher than 5 wt.% causes the carbon dioxide adsorption capacity to decrease lower than that of silica. This indicates the chemical phase transformation on the surface of silica forming an inactive material. With 5 wt.% K_2CO_3 loading only a small amount of potassium silicate is formed in the pores of the composite sorbents and the rest of the composite sorbents can still be utilized as shown in an slight increase in carbon dioxide adsorption capacity compared to that of silica. A low activity of the silica based sorbents probably derives from the large pore size of the silica, which lowers the dispersion of the impregnated salts. As a result, a further increase in K_2CO_3 loading causes the reduction in active composite sorbents (less pore volume, most of which were occupied by potassium silicate) due to the formation of inactive potassium silicate on the surface of silica, which results in a decrease in carbon dioxide adsorption capacity.

K_2CO_3-on-Al_2O_3

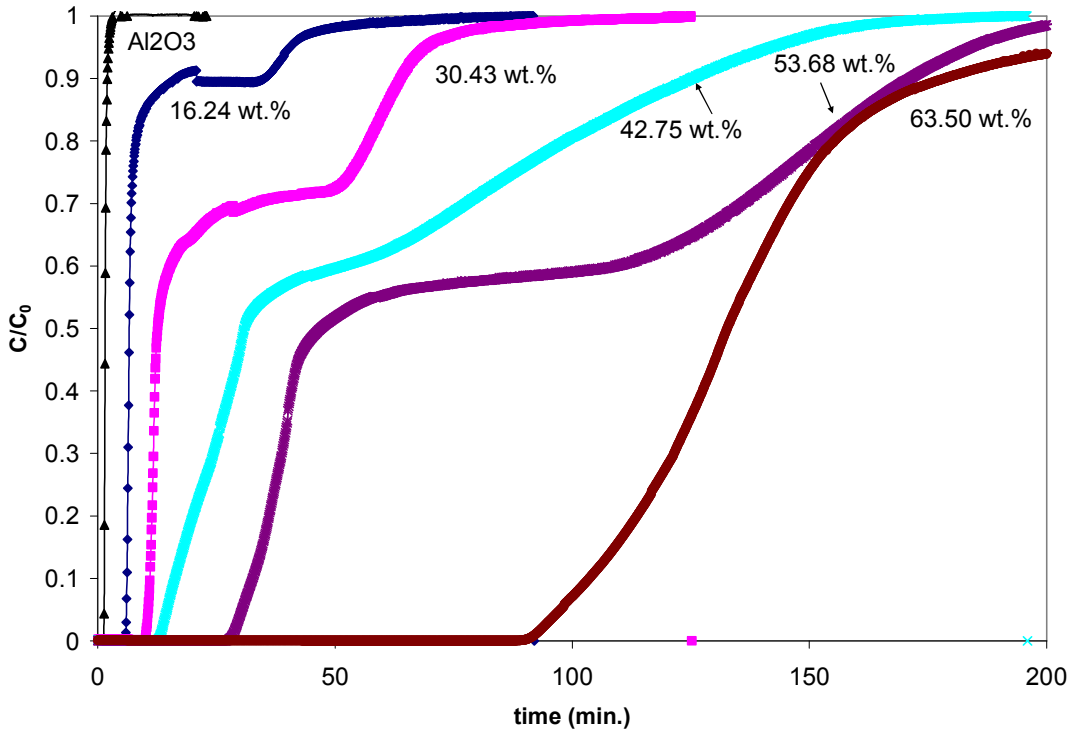

Figure 19: Breakthrough curves of K_2CO_3/Al_2O_3 at different K_2CO_3 loadings

Figure 19 shows the breakthrough curves of the Al_2O_3-composite sorbents at various K_2CO_3 loadings. The alumina composite sorbents show high carbon dioxide adsorption capacity compared to those of silica composite sorbents. The composite sorbents were observed to increase in volume after drying in the oven at 100^{o}C for 30 minutes. The carbon dioxide adsorption capacity was then calculated as a function of K_2CO_3 loading as shown in Figure 20.

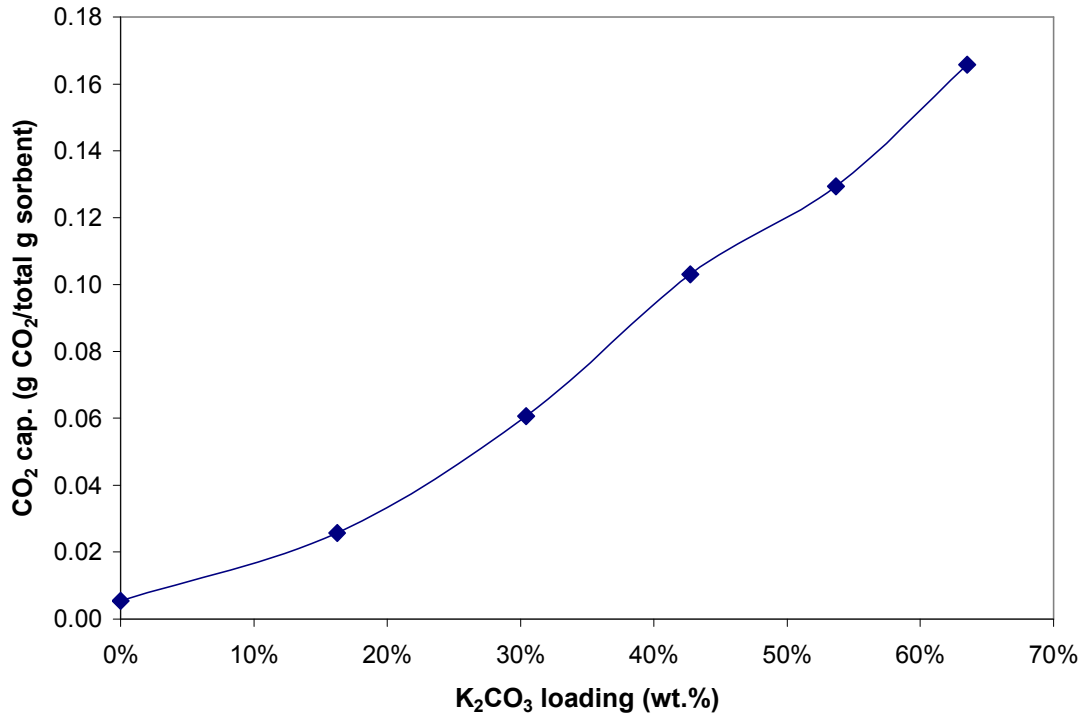

Figure 20: CO_2 adsorption capacity of Al_2O_3 composite sorbents as a function of K_2CO_3 loadings

Based on Figure 20, it is shown that an increase in K_2CO_3 loading shows an increase in carbon dioxide adsorption capacity. The composite sorbents can reach 0.17 g CO_2/total g of sorbent. These alumina based composite sorbents might be the best candidate for carbon dioxide adsorption application due to their high adsorption capacity. However, an increase in volume after drying might be due to chemical reaction between potassium carbonate and alumina causing a chemical phase transformation. As a result, the composite sorbents were then analyzed by XRD.

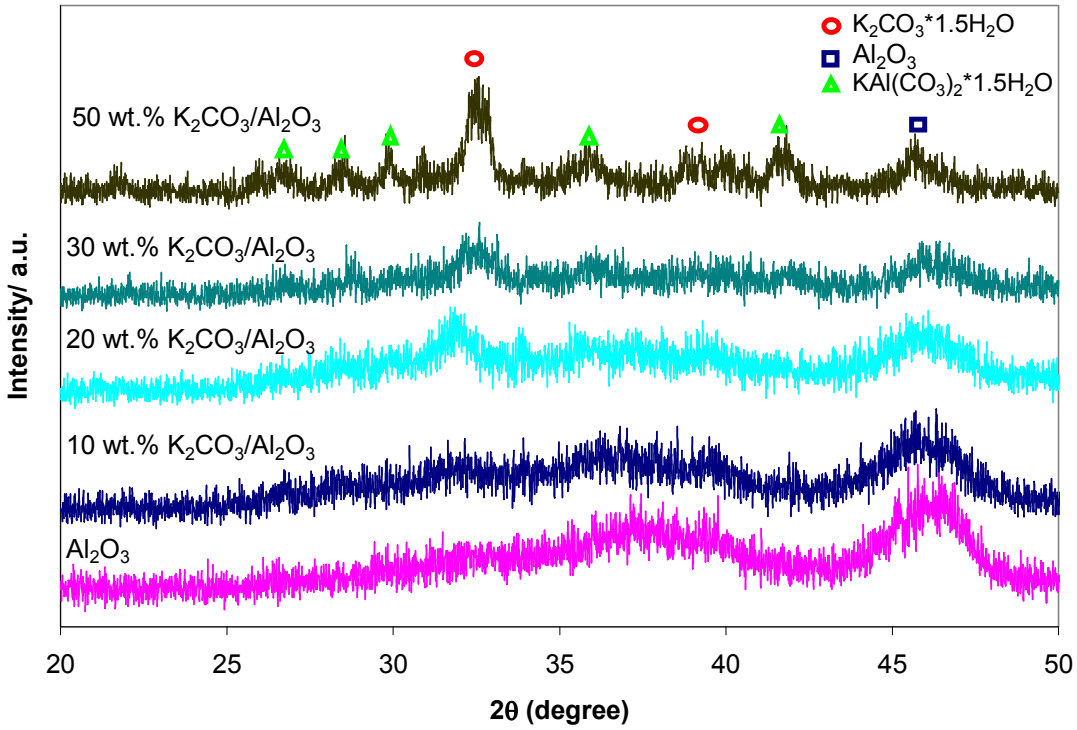

Figure 21: XRD patterns of Al_2O_3 and K_2CO_3 impregnated Al_2O_3 with different loadings

The XRD patterns in Figure 21 shows an amorphous nature of alumina particles as shown in the broad peaks between 35-40^o and 45-50^o respectively. Figure 21 shows that at 10 wt.% K_2CO_3, the XRD pattern of the composite sorbent is similar to that of the pure Al_2O_3 particles. This is due to the high dispersion of the K_2CO_3 in the porous matrix of alumina and the low K_2CO_3 loading resulting in no K_2CO_3 reflections detected. An increase in K_2CO_3 loading (>10 wt.%) leads to the mixture of the phase between Al_2O_3 (37^o) and K_2CO_3*1.5H_2O (32.4^o).

The K_2CO_3 can incorporate into the surface lattice of Al_2O_3 and diffuse into the bulk of Al_2O_3 with the formation of potassium alumino carbonate, but the reaction is limited by the amount of K_2CO_3 added due to the pore volume. Shaeronov et al [35]

investigated the same system and concluded that the K_2CO_3 and Al_2O_3 react at low temperature forming potassium alumino carbonate as shown in the following reaction:

$$xK_2CO_3 + yAl_2O_3 \Leftrightarrow xK_2O*yAl_2O_3*(x-y)CO_2 + yCO_2$$

At 10 wt.% K_2CO_3 loading, the formation of potassium alunino carbonate is confined in the pores of alumina and due to the low K_2CO_3 loading only a small amount of potassium alumino carbonate is formed. A further increase in K_2CO_3 loading promotes the formation of potassium alumino carbonate in the pores of alumina resulting in a decrease in pore volume. The reduction in pore volume causes a condensation of K_2CO_3(aq) out of the pores of alumina forming $K_2CO_3*1.5H_2O$(s). A further increase in K_2CO_3 loading causes more $K_2CO_3*1.5H_2O$ to precipitate as shown in a decrease in weaker Al_2O_3 reflections and stronger $K_2CO_3*1.5H_2O$ reflections. These precipitates react with CO_2 as shown in the following reaction:

$$K_2CO_3*1.5H_2O + CO_2 \rightarrow HCO_3^- + H^+ + K_2CO_3 + 0.5H_20$$

The amount of CO_2 adsorbed depends on the formation of potassium sesquihydrate. A result of additional K_2CO_3 loading causes potassium sesquihydrate to precipitate and yields higher CO_2 capacity. The process is not reversible. This transformation will be further discussed in Chapter VIII.

K_2CO_3-on-Activated Carbon Particles

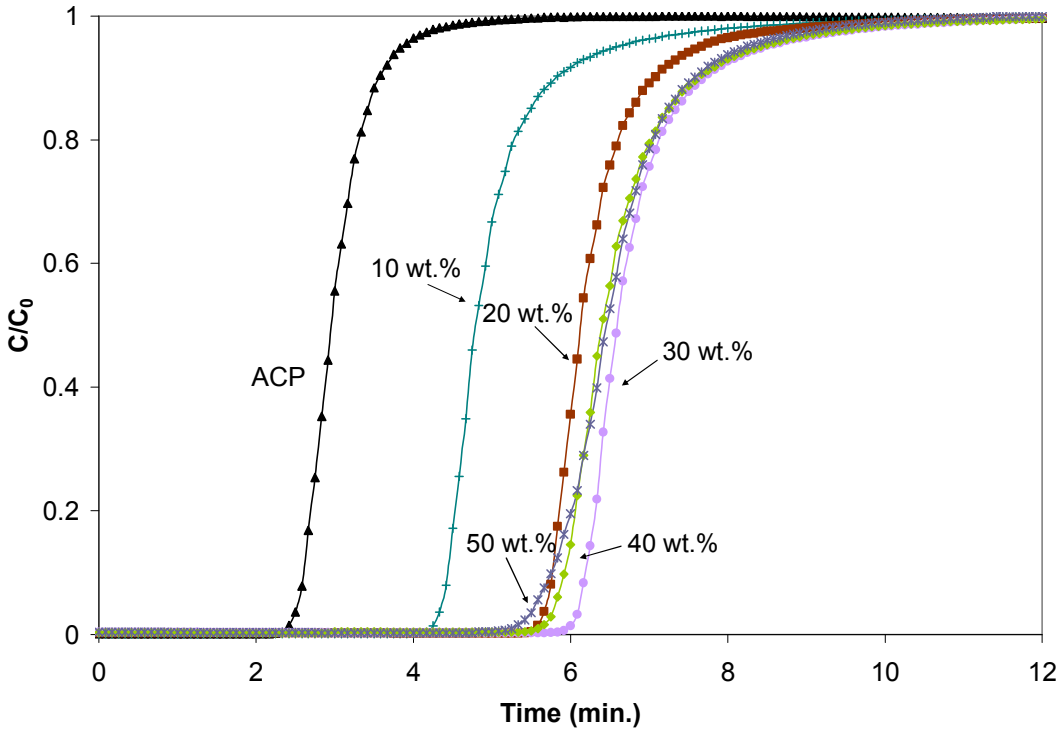

Figure 22: Breakthrough curves of K_2CO_3/ACP at different K_2CO_3 loadings

The ACP composite sorbents underwent breakthrough tests as shown in Figure 22. It was found that an increase in K_2CO_3 loading yields an optimal K_2CO_3 loading around 30 wt.%--- this composite sorbent can reach 0.01 g CO_2/total g of the sorbent and yield 30% utilization at room temperature. Unlike K_2CO_3/SiO_2 and K_2CO_3/Al_2O_3, an increase in volume after drying ACP composite sorbents at 100°C for 30 minutes of the K_2CO_3/ACP sorbents was not observed. The ACP composite sorbents yield higher carbon dioxide adsorption capacity than that of silica composite sorbents, but lower than that of alumina composite sorbents. The ACP composite sorbents show sharp breakthrough curves indicative of high utilization of the sorbents. This type of composite sorbents will be further discussed in Chapter VI.

Thermal stability

One of the most important attributes for adsorbents is the regenerability. To determine the regenerability and their mechanisms at elevated temperatures, spent K_2CO_3/ACP and K_2CO_3/Al_2O_3 composite sorbents were then tested by DSC at the heating rate of 10°C/min from 35 to 400°C as shown in Figure 23.

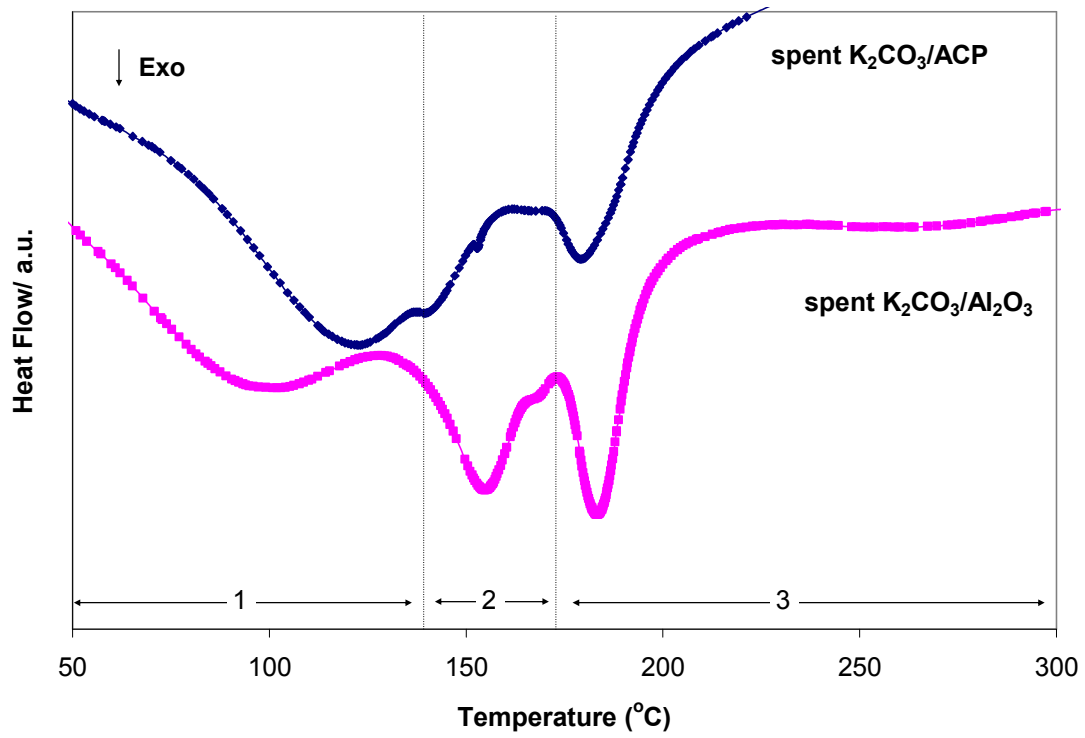

Figure 23: DSC spectra of spent K_2CO_3/ACP and K_2CO_3/Al_2O_3

1: removal of physically adsorbed water
2: side reaction
3: decomposition of $KHCO_3$ in Ar

It was found that the K_2CO_3/ACP sorbents exhibit three exothermic peaks. The first broad peak between 50 and 130°C is associated with the removal of physically adsorbed water. The second peak between 130-160°C is associated with the dehydration of

crystallization water in the composite sorbent. The third peak between 160 and 220^{o}C corresponds to the decomposition of $KHCO_3$. For K_2CO_3/Al_2O_3 sorbents, the DSC study exhibits similar phenomenon as the K_2CO_3/ACP sorbents. The DSC spectrum shows three exothermic peaks at 50-130^{o}C, 130-160^{o}C, and 170-220^{o}C corresponding to the removal of physically adsorbed water, dehydration of crystallization water, and decomposition of $KHCO_3$ respectively. However, the K_2CO_3/Al_2O_3 composite sorbent exhibits a strong exothermic reaction between 130 and 160^{o}C, which results from the reaction between $KHCO_3$ and Al_2O_3 as follows:

$$2xKHCO_3 + yAl_2O_3 \Leftrightarrow xK_2O*yAl_2O_3*(x-y)CO_2 + (x+y)CO_2$$

The product of this reaction is inactive and it will be further discussed in Chapter VIII.

Summary:

The nature of the host matrix has a strong influence on the CO_2 adsorption capacity and sorbent regenerability. The use of three host matrix supports shows an increase in CO_2 adsorption capacity in a sequence: SiO_2<ACP<Al_2O_3. Even though the use of Al_2O_3 as support materials offers higher CO_2 adsorption capacity than that of ACP and SiO_2, a hydrothermal reaction between Al_2O_3 and K_2CO_3 takes place around 100^oC causing K_2CO_3*1.5H_2O to precipitate out of the pores of alumina. These precipitates are associated with the decomposition of $KHCO_3$ around 150^oC and result in formation of an inactive material as shown in the following mechanisms:

$xK_2CO_3 + yAl_2O_3 \Leftrightarrow xK_2O*yAl_2O_3*(x-y)CO_2 + yCO_2$

$2xKHCO_3 + yAl_2O_3 \Leftrightarrow xK_2O*yAl_2O_3*(x-y)CO_2 + (x+y)CO_2$

As a result, the K_2CO_3/Al_2O_3 sorbents are not suitable for regeneration as the CO_2 adsorption capacity gradually decreases from the reaction between Al_2O_3 and K_2CO_3 and $KHCO_3$. Due to its high carbon dioxide adsorption capacity, the Al_2O_3-composite sorbents have a potential for a single-use carbon dioxide removal in a humid gas where molecular sieves can not be utilized.

IV. BREAKTHROUGH PERFORMANCE OF K_2CO_3/ACP SORBENTS AND THEIR REGENERABILITY

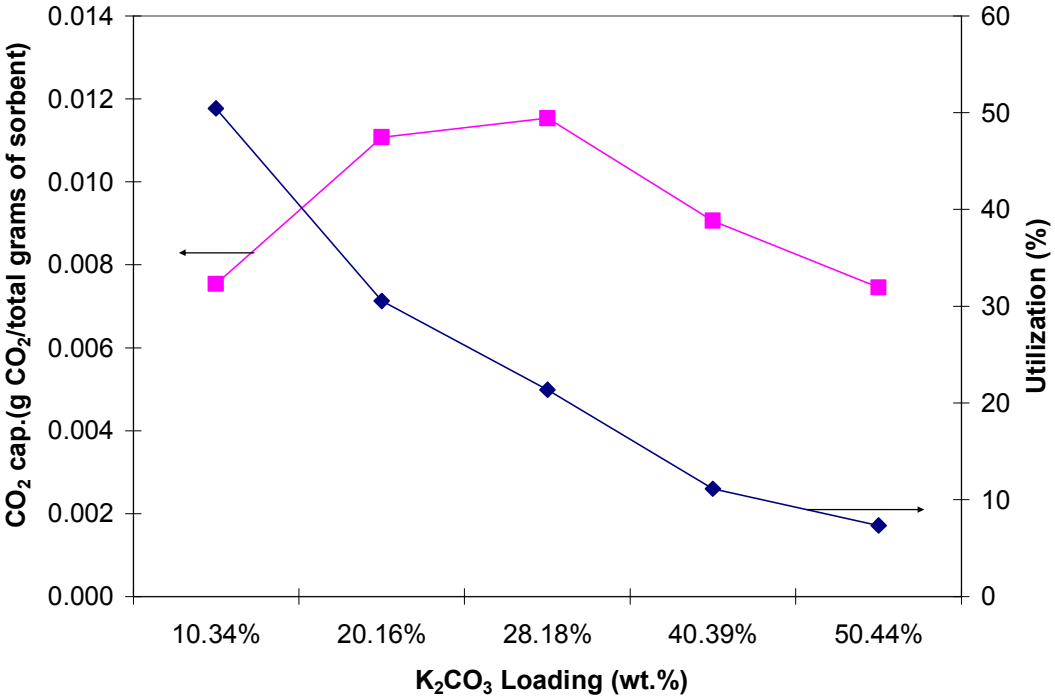

Figure 24: CO_2 adsorption capacity and utilization of K_2CO_3/ACP sorbents at different K_2CO_3 loadings

The carbon dioxide adsorption capacity was calculated from the breakthrough curves in Figure 24. The CO_2 adsorption capacity of ACP-based sorbents can reach 0.012 g CO_2/ total gram of sorbents with the utilization of 30% as shown in Figure 24.

This type of sorbents can be used in a large adsorber or in the processes that have many adsorbers as the saturated bed can undergo regeneration while using other adsorbers for adsorption.

The low carbon dioxide adsorption capacity resulted from the high porosity of activated carbon particles (0.48 g/cc.); however, this high porosity of ACP helps to disperse chemically active compound (K_2CO_3) in the pores, enhances the accessibility, and lowers regeneration temperatures. This section shows a study of K_2CO_3/ACP sorbents to reveal characteristics of the sorbents.

Effect of moisture content on the CO_2 capacity of the sorbents

Based on equation 1 in Chapter II, water is necessary as it is one of the reactants. It was found that additional water enhanced the performance of the sorbents; however, it was not very well understood. In this section, three aspects of additional water are investigated: excess water (free water), crystallization water, and water from gas stream. A series of breakthrough experiments was conducted to understand the mechanism.

Effect of crystallization water

Figure 25 shows breakthrough tests of 5g of pure K_2CO_3 in dry and wet conditions. The breakthrough curve of the sorbent under dry condition shows no carbon dioxide adsorption capacity (residence time = 0.5 min). The challenge gas was then by-passed through a H_2O saturator prior to entering the adsorber and the breakthrough result

shows an increase in carbon dioxide adsorption capacity compared to that of the dry condition.

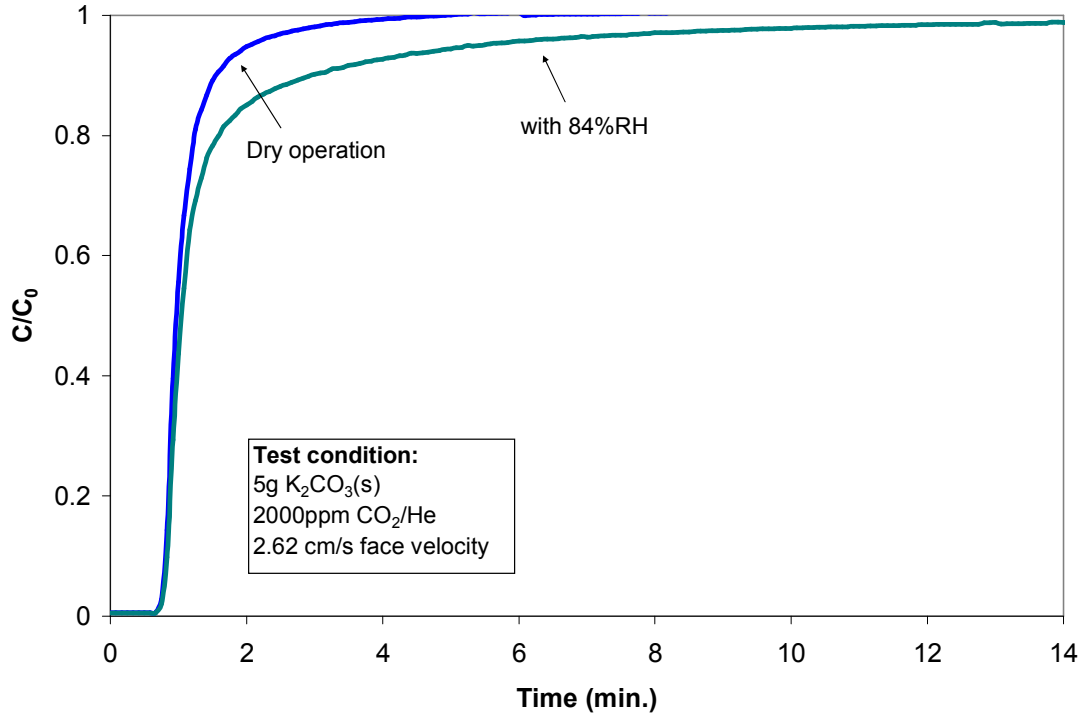

Figure 25: Breakthrough curves of K_2CO_3 in dry and wet gas streams

The adsorption of carbon dioxide by potassium carbonate takes place in the surface layer of water formed by moisture carried by gas stream and the remaining water in the sorbents. Carbon dioxide diffuses in the water layer and is neutralized by the dissolved K_2CO_3 shown in the following reactions:

$H_2O + CO_2 \Leftrightarrow H_2CO_3$

$H_2CO_3 \Leftrightarrow H^+ + HCO_3^-$

$HCO_3^- \Leftrightarrow H^+ + CO_3^{2-}$

$2H^+ + CO_3^{2-} + K_2CO_3 \Leftrightarrow 2KHCO_3$

The solid K_2CO_3 sorbents do not adsorb carbon dioxide; however, they can create a water environment by dissolving in the water layer and reacts with carbon dioxide. As a result, the solubility of the K_2CO_3 (shown in Table 14) in this water surface determines the carbon dioxide adsorption capacity and the rate of adsorption. An addition of water from the gas stream forms a water layer at the surface of the sorbents, but the hydration reaction is kinetically slow as shown in the breakthrough curves. It is shown that an insufficient of crystallization water results in an additional step in order to add water molecules (create water environment). This is more likely a rate-determining step.

$K_2CO_3 + xH_2O \rightarrow K_2CO_3{*}xH_2O$

Effect of remaining water during sorbent preparation

The prepared sorbents were dried in the vacuum oven at 100°C at different drying times. The influence of drying time is to determine the remaining water in the sorbents. The maximum CO_2 adsorption capacity corresponds to the x/K ratio of 16 as shown in Figure 26.

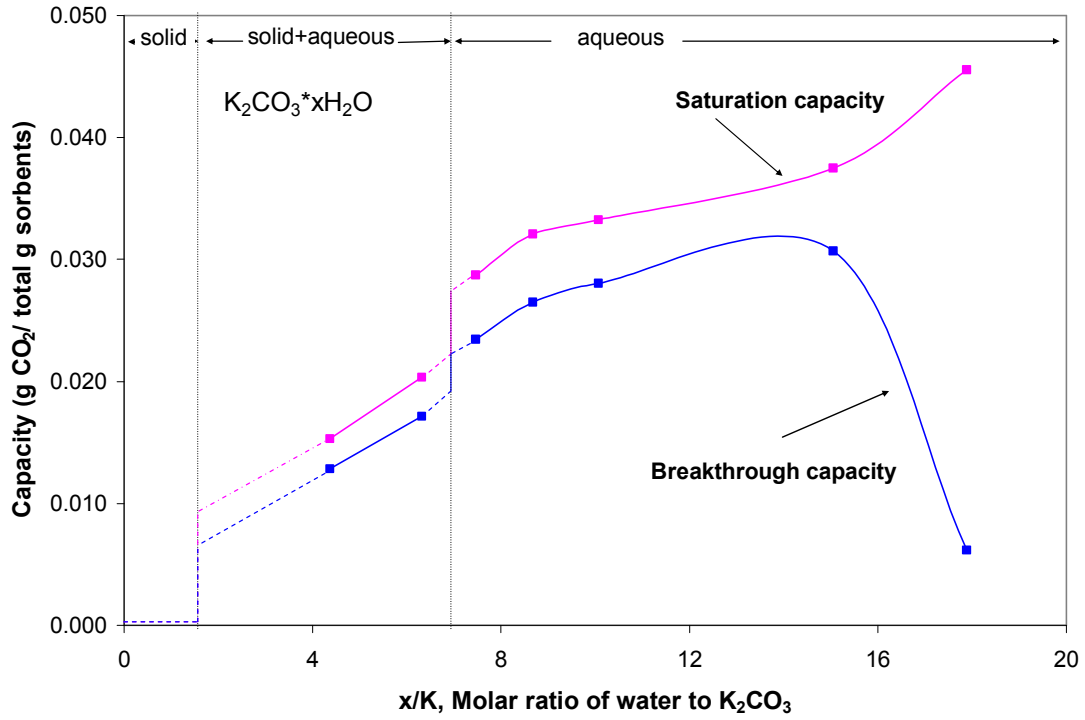

Figure 26: CO_2 adsorption capacity at various moisture contents

The x/K ratios show the state of the sorbents in the porous support matrix. Based on the solubility and liquid density of K_2CO_3 as shown in Table 14, it is found that at x/K ratio of 1.5 and lower, the sorbents are in the solid state and yield low carbon dioxide adsorption capacity. An increase in x/K ratios between 1.5 and 7, a part of K_2CO_3*xH_2O dissolves in the additional water in the system and results in the mixture between solid and aqueous phase, which offers higher carbon dioxide adsorption capacity than those

with lower x/K ratios. A further increase in x/K ratios higher than 7.5 causes all K_2CO_3*xH_2O to dissolve in the water addition as evidenced by the solubility limit of K_2CO_3. At this state, the composite sorbents offer highest carbon dioxide adsorption capacity. Figure 27 shows the schematic of the composite sorbents in the ACP porous matrix.

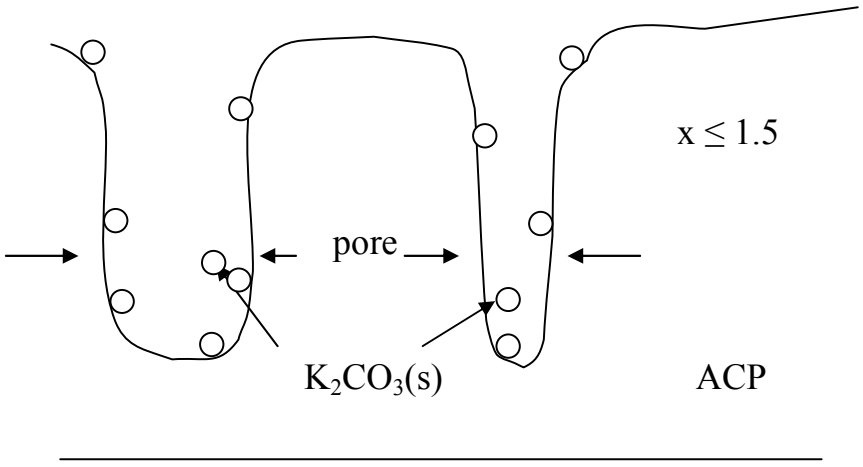
x ≤ 1.5
pore
K_2CO_3(s)
ACP

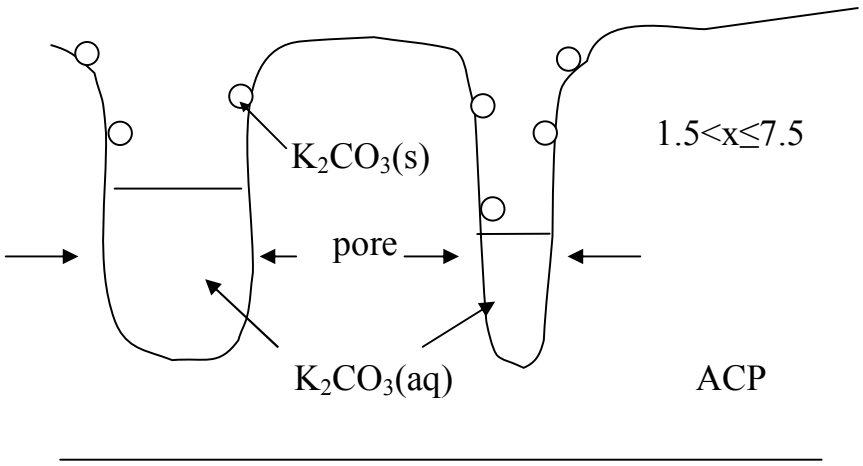
1.5<x≤7.5
K_2CO_3(s)
pore
K_2CO_3(aq)
ACP

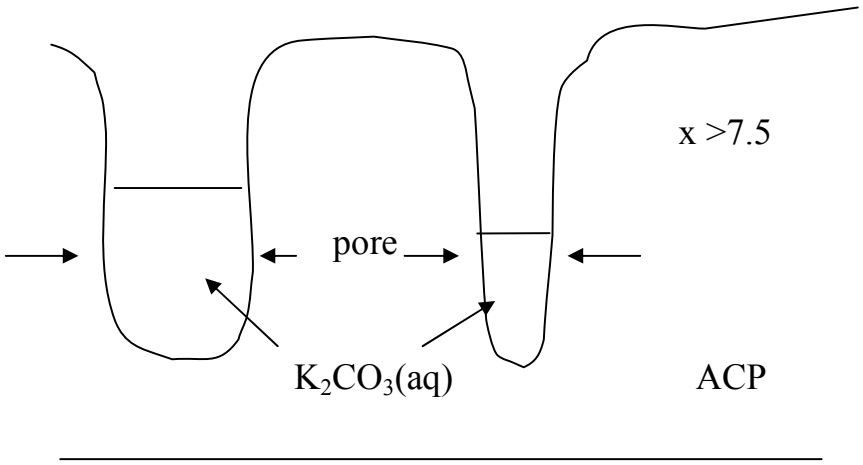
x >7.5
pore
K_2CO_3(aq)
ACP

Figure 27: Schematic phase diagram of K_2CO_3 in the pores of activated carbon

Table 14: Solubility and liquid density of K_2CO_3 and $KHCO_3$ at 25°C

	Solubility (g solute/1000 g water)	Saturation density (g/cc.)
K_2CO_3	1126	1.145
$KHCO_3$	333	1.165

In this study, the water layer on surface comes from remaining water in sorbents with different drying times. The phase of the sorbents is controlled by the solubility limit of K_2CO_3 and the amount of water remained after drying. The composite sorbents need to create a water environment (water surface layer), in which carbon dioxide adsorption takes place. The carbon dioxide from gas stream diffuses in the water layer forming carbonic acid and allows chemisorption between carbon CO_2 and K_2CO_3(aq). If the water environment is not created, the hydration is the rate-determining step. An insufficient water (x/K < or =1.5), the K_2CO_3 is in the form of solid, which needs to be dissolved in the water in the surface layer to capture carbon dioxide. An increase in the x/K ratios between 1.5 and 7 (additional water) causes a partial K_2CO_3 to be dissolved in water (create water environment) and presents in a mixed phase between solid and aqueous. The K_2CO_3 in water environment can readily react with carbon dioxide while the K_2CO_3(s) needs to create a water environment by dissolving in the water surface, which results in higher carbon dioxide adsorption capacity than those with x/K ratio lower than 1.5. A further increase in x/K ratios beyond 7 causes all K_2CO_3 to dissolve

and readily react with carbon dioxide resulting in an increase in carbon dioxide adsorption capacity.

Effect of additional water

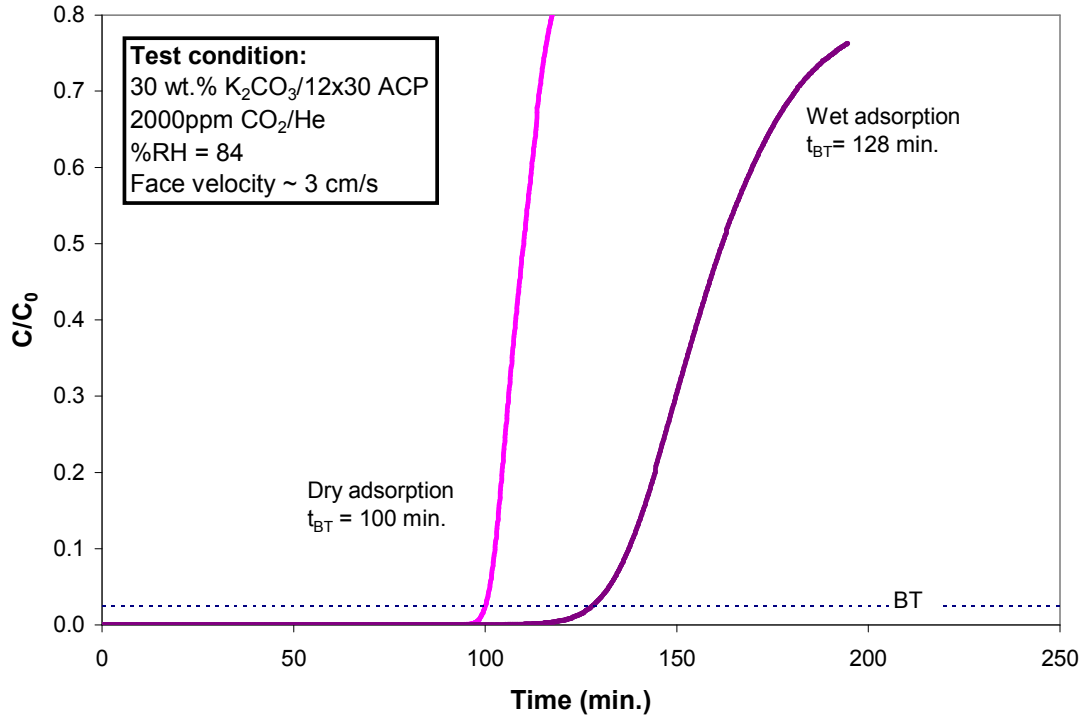

Figure 28: Breakthrough curves of K_2CO_3/ACP in dry and wet gas streams

In the previous section, it was shown that additional water from the gas stream in order to maximize the formation of HCO_3^- to enhance the CO_2 adsorption capacity depends on the state of the composite sorbents. Those sorbents in the aqueous form exhibit higher CO_2 adsorption capacity than those in solid or mixture between solid and liquid.

The K_2CO_3/ACP sorbents were tested under wet and dry conditions. The composite sorbents possess x/K ratio of 16 indicative of water layer formation, which is

readily adsorbs carbon dioxide in the water layer. It is shown in Figure 28 that the additional water from gas stream shows 28% increment in breakthrough capacity. The state of the composite sorbents determines the rate of intermediate formation (HCO_3^-) in the surface layer. Since the water layer is already formed by water adsorption from the sorbent, additional water adsorption from the gas stream should not have any effect on the carbon dioxide adsorption capacity. In effect, additional water from gas stream might dilute the K_2CO_3(aq) in the composite sorbents and result in a drop in carbon dioxide adsorption capacity. However, an increase in breakthrough and saturation capacity of CO_2 was observed as seen in the shift of the breakthrough curve to the right side in Figure 28. The high x/K ratio of the current composite sorbent indicates the amount of HCO_3^- formed in the surface layer and results in rapid formation of $KHCO_3$. Based on the difference in solubility and liquid density of K_2CO_3 and $KHCO_3$, precipitation of $KHCO_3$ is expected and the precipitation of $KHCO_3$ hinders the composite sorbents from being fully utilized. As a result, the additional water adsorption from the gas stream stabilizes the formation of $KHCO_3$ from precipitation as seen in an increase in breakthrough time from 100 minutes to 128 minutes.

Determination of regeneration temperature

The DSC and thermodynamic calculation using HSC chemistry [36] were utilized to determine the decomposition of the $KHCO_3$. The change in δG normally indicates the possibility of reverse reaction to take place. It is found that there is a change in δG around 167°C indicative of decomposition of $KHCO_3$ forming K_2CO_3 as shown in Figure 29.

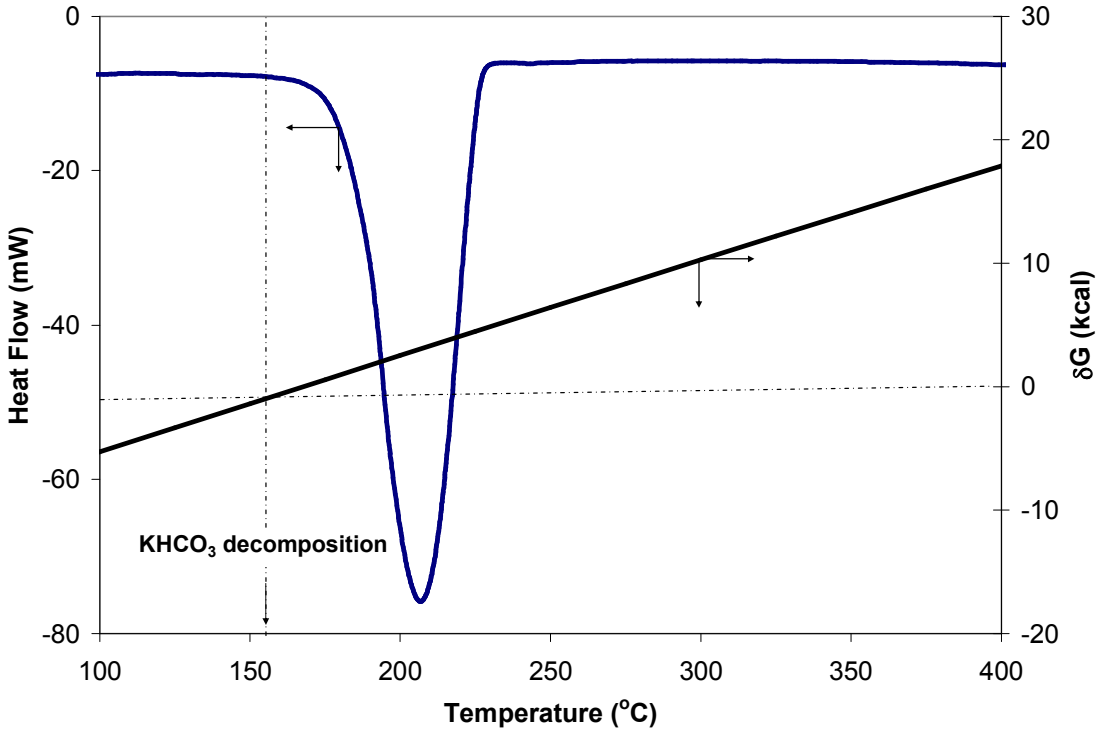

Figure 29: DSC spectrum and calculated δG as a function of temperature

The DSC experiment was conducted using bulk $KHCO_3$ with the heating rate of 10°C/min from 35°C to 500°C. The DSC spectrum exhibits one exothermic peak with an onset around 150°C, which confirms the possible decomposition of $KHCO_3$ at 150°C.

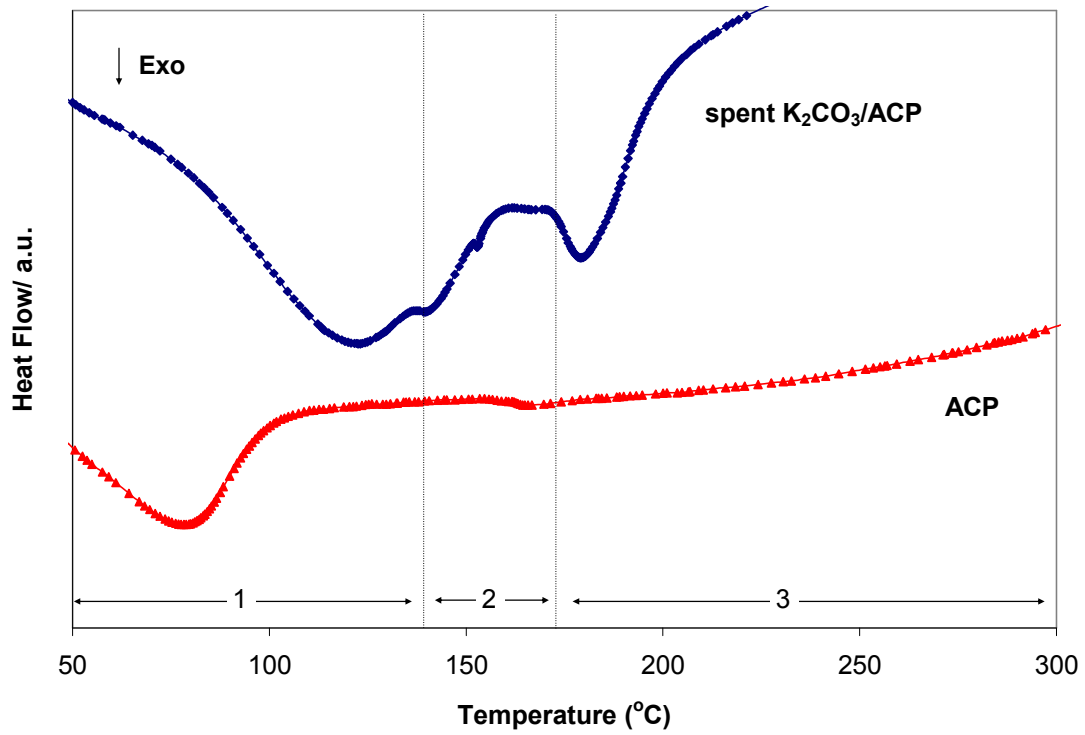

Figure 30: DSC spectra of ACP and K_2CO_3 impregnated ACP

The spent ACP composite sorbents were then tested by DSC. The result of the spent ACP composite sorbents shows three exothermic peaks as shown in Figure 30. The first broad peak between 50 and 130°C is associated with the evaporation of physically adsorbed water. The same broad peak was observed in the ACP particulate samples. The second peak between 130 and 169°C was observed. This peak is associated with the dehydration of crystallization water. The third peak between 169 and 223°C corresponding to the decomposition of $KHCO_3$. The spent composite sorbents were then regenerated at 150°C and tested for carbon dioxide adsorption characteristics.

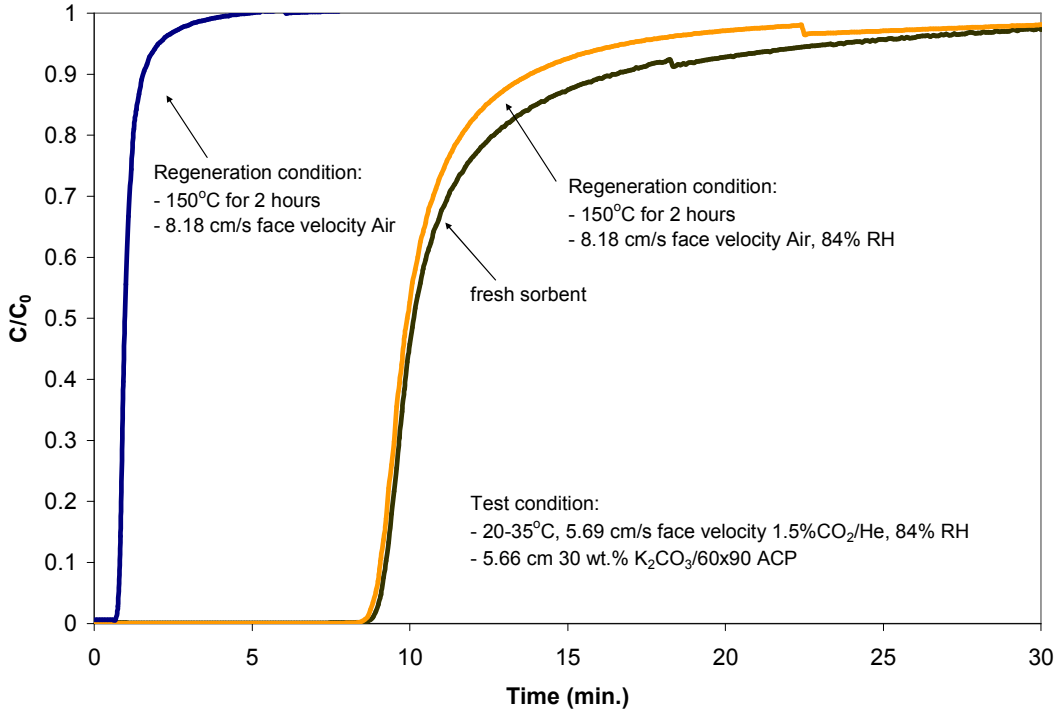

Figure 31: Breakthrough curves of K_2CO_3/ACP in wet and dry regeneration conditions

Figure 31 shows the breakthrough curves of the freshly prepared composite sorbent and spent composite sorbents regenerated in steam and dry air. It is shown that the regeneration in steam restores 98% carbon dioxide adsorption capacity of the fresh sorbent. However, carbon dioxide adsorption capacity of the composite sorbent regenerated in dry air was not restored. The regeneration in dry air at 150°C for two hours causes the sorbents to lose remaining water in the sorbents and also the crystallization water forming a non-reactive K_2CO_3(s) in the porous matrix. The presence of K_2CO_3 in the composite sorbents after regeneration in dry air is confirmed by XRD pattern as shown in Figure 32. This reaction product, K_2CO_3 is inactive compared

to the initial potassium carbonate. The additional water can be added from the gas stream to form a water layer, but hydration reaction is kinetically slow at room temperature. As a result, the water is rather necessary during regeneration to maintain the water layer and prevent K_2CO_3(s) formation.

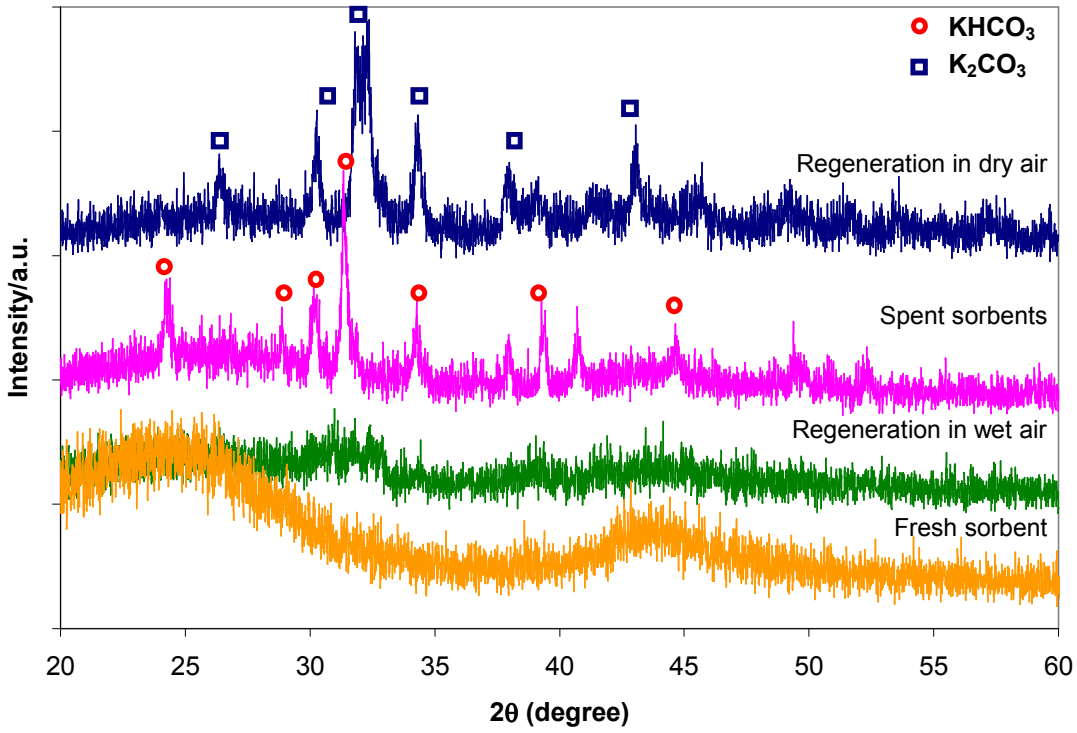

Figure 39: XRD patterns of K_2CO_3/ACP sorbents under wet and dry regeneration conditions

The XRD patterns of the fresh composite sorbent and ACP shows similar feature. This indicates the presence of K_2CO_3(aq) in the porous matrix of ACP. Adsorption of carbon dioxide on the composite sorbents results in the formation of potassium bicarbonate as shown in the presence of $KHCO_3$ peaks on the spent composite sorbent. The spent

sorbents were then regenerated in dry and wet air. The one regenerated in steam shows similar feature as a fresh sorbent indicative of the decomposition of $KHCO_3$ and the formation of K_2CO_3(aq). The composite sorbent regenerated in dry air shows a presence of an inactive K_2CO_3(s).

V. MICROFIBROUS MEDIA AND ITS APPLICATIONS

For the removal of carbon dioxide at low temperature, adsorption technology is currently limited to inefficient packed bed adsorption. To date, high levels of adsorption are achieved by a thick and series of packed beds of molecular sieves for multicyclic adsorption and desorption with additional packed beds of silica to remove moisture in order to ensure the high activity of the carbon dioxide adsorption beds. Another technology utilizes the single-use packed beds of Sodalime. This type of sorbents often uses in medical and military applications in a thick, single-use packed beds. The use of large particulates lowers the adsorption capacity and efficiency while maintaining lower pressure drop than that of the packed beds of small particulates. Several new technologies including membrane processes and cryogenic processes are in development but none are operational readiness due to its high investment cost. An optimized composite bed system is designed to meet a series of specific objectives for carbon dioxide removal performance unattainable by current packed bed adsorbers or new competing technologies.

Microfibrous Media

K_2CO_3/ACP particulates of 150-250 μm were uniformly entrapped into a sinter-locked 3-dimensional network of 12 and 8 μm nickel fibers. The use of small particulates significantly attenuates the intraparticle diffusion limit. The sinter-locked matrix of microfibrous media enhances the external mass transfer, which promotes high log contacting efficiency in a thin layer. SEM micrograph in Figure 33 shows microstructure of the thin microfibrous entrapped K_2CO_3/ACP sorbents for CO_2 adsorption.

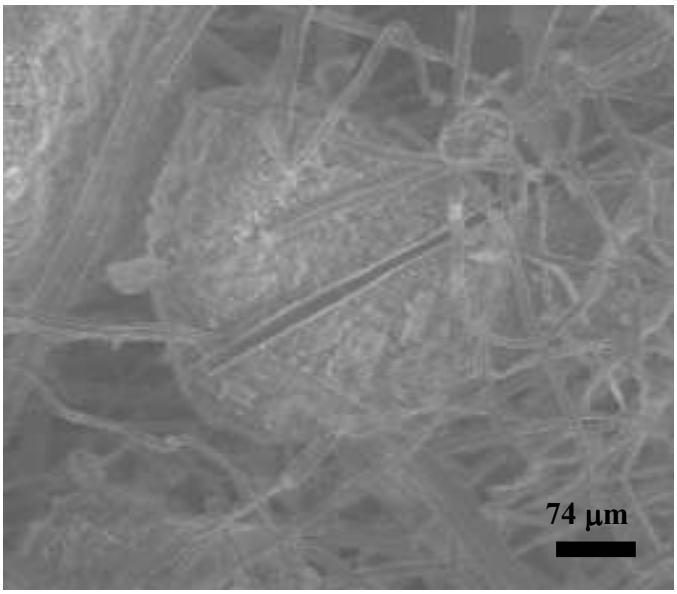

Figure 33: SEM micrograph of microfibrous media

As shown in Figure 33, the nickel fibers partially melt during sintering and formed a fiber network in a cage-like matrix to entrap activated carbon particulates inside. This network holds the composite sorbents from moving during adsorption and

desorption. As a metal, nickel fibers possess high thermal conductivity compared to other types of fibers (i.e. polymer fibers), which enhances the thermal contacting and reduces the regeneration time due to a uniform heat distribution during regeneration.

Composite Bed

The microfibrous media (MM) can be used as a stand alone or in a composite bed. The composite bed utilizes the microfibrous media as a polishing sorbent layer to back up a packed bed that suffers from high intraparticle mass transfer resistance and low contacting efficiency. The concept of the composite bed is to enhance the external mass transfer while reducing internal mass transfer resistance, all of which maximize the breakthrough capacity of the composite bed per unit volume and lower the thermal effects (i.e. regeneration temperature and heat of reaction) as well as pressure drop.

A composite bed consisting of packed bed of K_2CO_3/ACP sorbents (1mm. pellet) followed by microfibrous entrapped K_2CO_3/ACP polisher was tested. Figure 34 shows the schematic diagram of a series of the breakthrough tests for carbon dioxide adsorption of microfibrous media, a packed bed of K_2CO_3 impregnated ACP (1 mm pellet), and the composite bed.

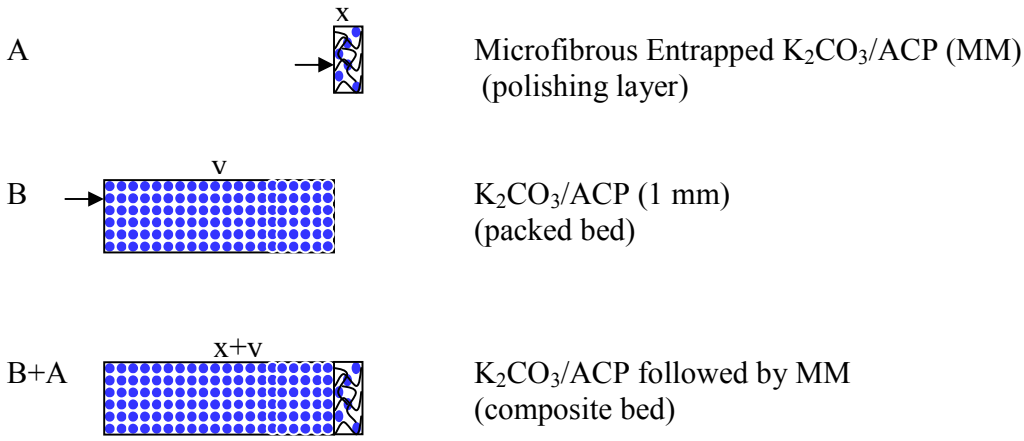

Figure 34: A schematic of a composite bed design (not to scale)

The microfibrous media with the thickness of 1.7 cm (x) and the packed bed of ACP composite sorbents with the bed thickness of 5.6 cm (v) are tested for its carbon dioxide adsorption capacity. The breakthrough curves are shown in Figure 35. The Figure 35 shows the comparison of the composite bed and a packed bed of the ACP composite sorbents.

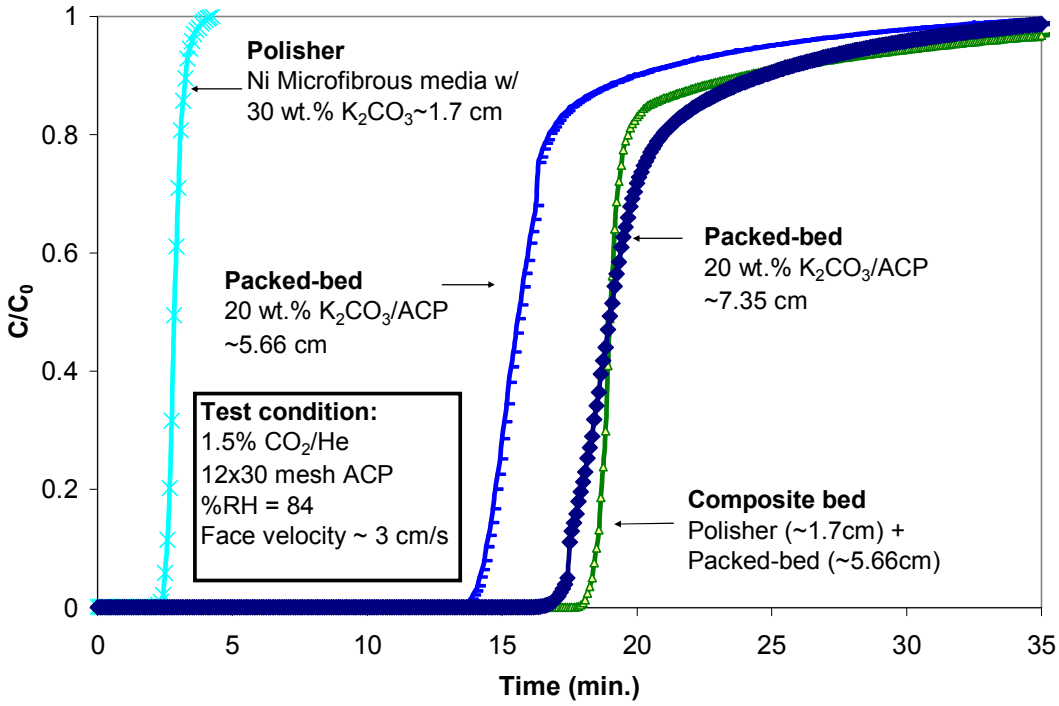

Figure 35: Comparative BT curves of a composite bed and a packed bed

It is shown that the composite bed offers higher breakthrough capacity compared to that of the packed bed. However, the improvement from microfibrous media was not pronounced due to the nano-dispersed nature of the packed bed of the prepared composite sorbents as shown in the calculated data in Table 15.

Table 15: Adsorption characteristics of composite sorbents

	Weight	Volume	CO_2 Adsorption Capacity (g CO_2/ total g sorbent)		Rate of adsorption
	g	cc	Breakthrough	Saturation	min^{-1}
Polisher	1.500	3.00	0.0189	0.0224	8.9809
Packed Bed	7.232	12.99	0.0175	0.0202	1.9165
Composite Bed	7.093	13.00	0.0233	0.0254	5.2188

It was found that a composite bed offers higher carbon dioxide adsorption capacity than that of the packed bed of the same volume. Moreover, the breakthrough curve of the composite bed is sharper than that of packed bed indicative of higher sorbent utilization with 63% higher in adsorption rate constant. The higher the adsorption rate constant indicates the faster the adsorption of carbon dioxide by the composite bed.

Regenerability of Microfibrous Media

To ensure the regenerability of the microfibrous media, the composite bed was then regenerated in steam at 150°C for two hours. The multicyclic breakthrough tests are shown in Figure 36.

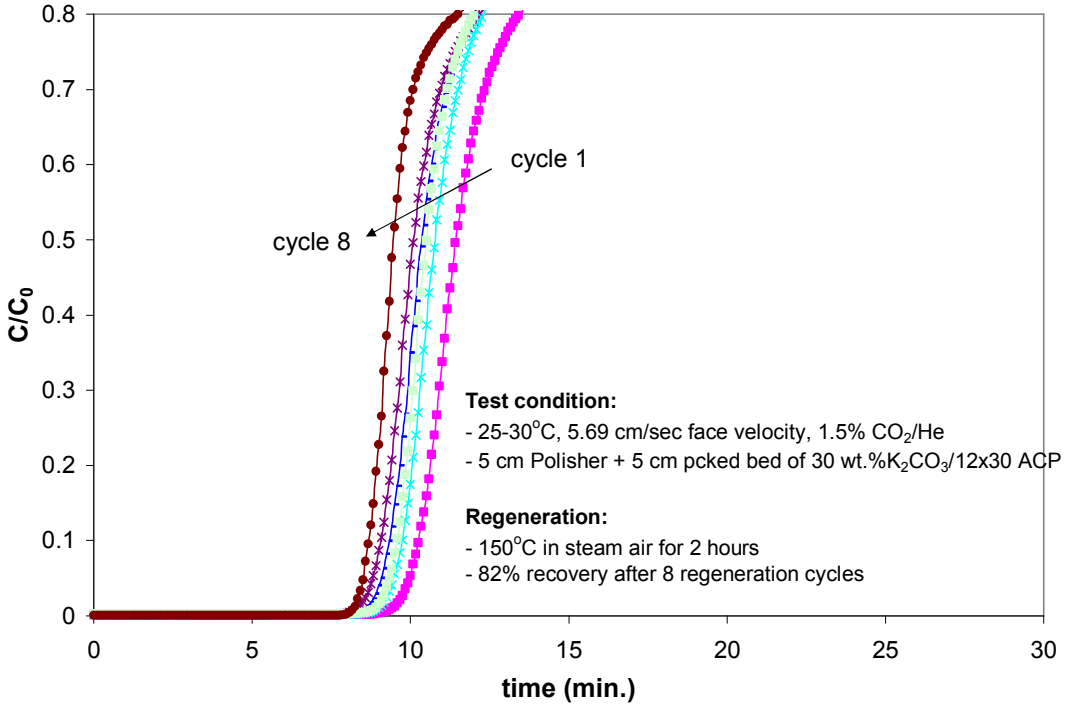

Figure 36: BT curves of composite beds from cycle 1 to cycle 8

The breakthrough results suggested that microfibrous entrapped K_2CO_3/ACP sorbents yield high regeneration ability as seen in the 84% recovery in CO_2 adsorption capacity after eight regeneration cycles. The reduction in CO_2 adsorption capacity is due to the formation of monohydrated potassium carbonate $K_2CO_3*H_2O(s)$ and/or anhydrous potassium carbonate $K_2CO_3(s)$---$K_2CO_3*1.5H_2O$ loses 5.59% of water at 100°C forming $K_2CO_3*H_2O$ and loses all the crystallization water in the range of 130-135°C [37].

However, the dehydration reaction of K_2CO_3*1.5H_2O is kinetically slow. As a result, the regeneration temperature has to be optimized in order to yield high utilization.

SEM micrographs in Figure 37 show the microstructure of the fresh microfibrous entrapped K_2CO_3/ACP sorbents and microfibrous media after eight regeneration cycles. No significant structural changes were observed in the sinter-locked network of the microfibrous media indicative of the robustness and high structural integrity.

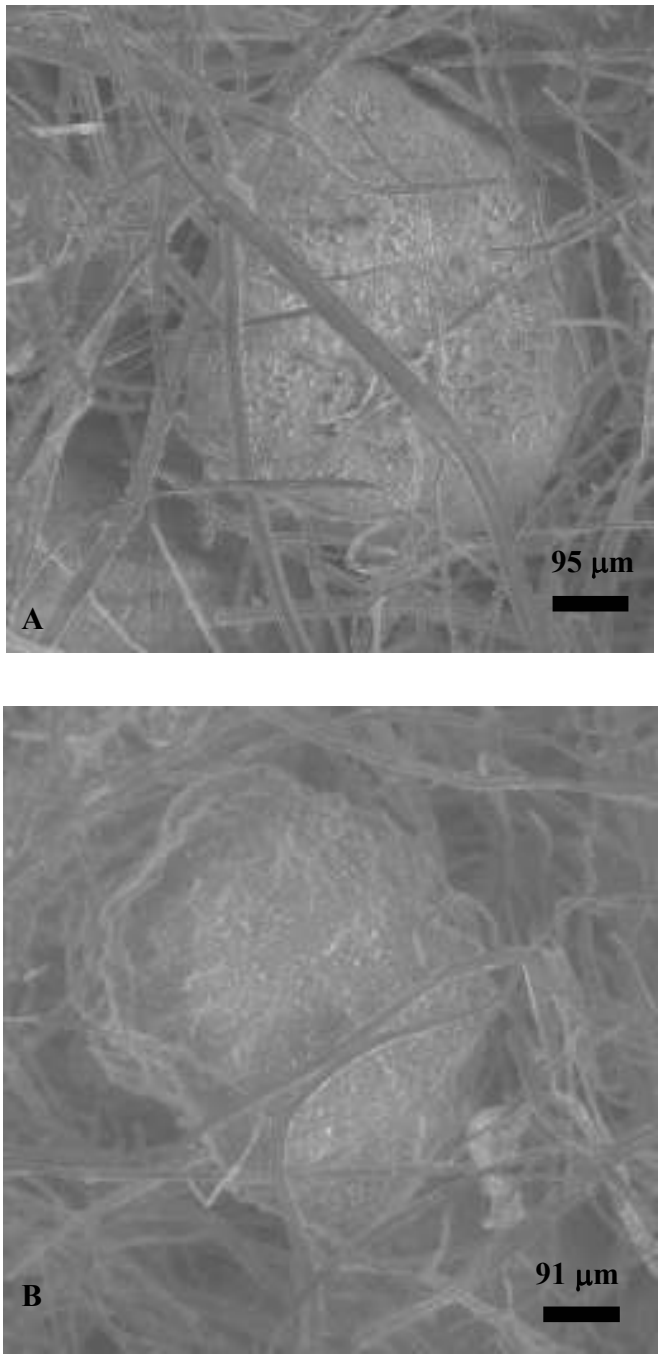

Figure 37: SEM micrographs of microfibrous media
A: fresh polisher
B: spent polisher after eight cycles of regeneration

Applications of polisher on Sodalime®

Sodalime is one of the commercially available solid sorbents for CO_2 adsorption. The main application is to use as a packed bed in a scrubber built into ventilation systems for cleaning closed-circuit breathing systems for military and medical applications [38]. The sorbents are $Ca(OH)_2$- based sorbents obtained from Molecular Products (UK). This type of sorbents often used in the submarine. The concept of the composite bed was then applied by using a polishing sorbent (~0.5 g/0.5 cm) backing up five grams of Sodalime®. The breakthrough tests were conducted and the results are shown in Figure 38.

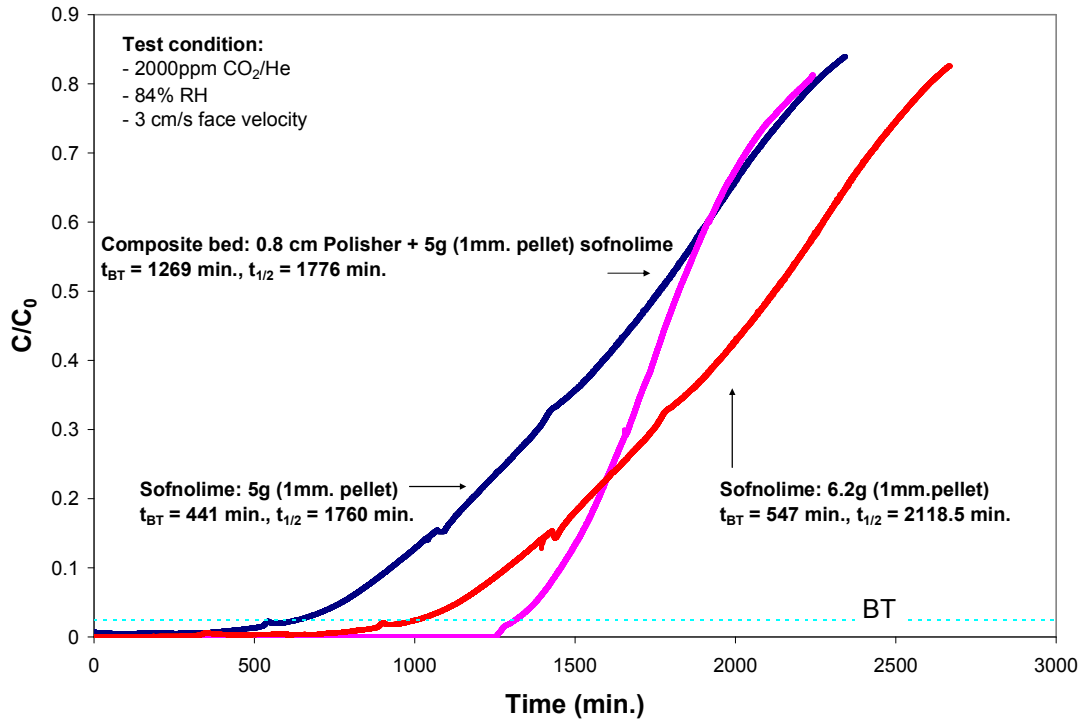

Figure 38: BT curves of composite bed using Sodalime®

From the breakthrough data, it was found that the composite bed shows higher carbon dioxide adsorption capacity and sharper breakthrough curve compared to that of the packed bed. The carbon dioxide adsorption capacity and adsorption rate constant were then calculated as shown in Table 16.

Table 16: Characteristics of Sofnolime in a composite bed design

	Mass	Volume	CO_2 Adsorption Capacity (g CO_2/ total g sorbent)		Rate of adsorption
	g	cc	Breakthrough	Saturation	min^{-1}
Packed Bed	6.2	7.38	0.091	0.624	0.0033
Composite Bed	5.5	7.84	0.240	0.646	4.4614

It is shown that the composite bed yields 120% higher breakthrough capacity with 90% higher adsorption rate constant than that of the packed bed of the Sodalime alone. These results indicate the advantages of using microfibrous media in a composite bed. At the same volume, the composite bed offers a sharper breakthrough curve than that of the packed bed indicating that microfibrous media not only helps the packed bed of poor sorbent utilization, but also reduce the critical bed depth resulting in reduction of adsorber size and volume.

Summary:

A regenerable microfibrous entrapped K_2CO_3/ACP sorbents has been developed and evaluated for CO_2 adsorption applications at room temperature. The use of microfibrous media in a composite bed combines the advantage of high volume loading of active sorbents from packed beds and the overall contacting efficiency of small particulates while minimizing the internal mass transfer resistance from a stand alone packed bed. The microfibrous media showed its ability to recover CO_2 adsorption capacity up to 86% after 8 regeneration cycles. The advantage of a low temperature reversible liquid phase absorption in an "apparent solid matrix" is as follows:

- High log contacting efficiency in a thin, low pressure drop media
- Low thermal effects (low regeneration temperature and δH of reaction)
- Capability to use as a stand alone of in a composite bed to obtain maximum capacity per unit volume
- Opportunity to use this approach on a low concentration and more sensitive applications (i.e. Metal-air batteries)

VI. STUDIES ON THE FORMATION OF THE SOLID SOLUTION COMPOUND IN K_2CO_3 IMPREGNATED AL_2O_3 SORBENTS

K_2CO_3 impregnated Al_2O_3 samples were prepared at various K_2CO_3 loadings. It was found that the Al_2O_3-based sorbents yield higher CO_2 adsorption capacity than ACP- and SiO_2-based sorbents. The breakthrough tests of these Al_2O_3-based sorbents reach 0.167 g CO_2/total g of sorbent with 80% utilization. The sample was then treated with steam at 150^oC in an adsorber, an increase in pressure drop was observed due to the formation of the big clusters along the wall of the adsorber. Unlike the K_2CO_3/ACP sorbents, the K_2CO_3/Al_2O_3 sorbents can not be regenerated due to its hydrothermal reaction between K_2CO_3 and Al_2O_3 at 100^oC causing formation of an inactive material, potassium alumino carbonate. As a result, DSC and XRD analyses were employed to understand this transformation.

XRD patterns in Figure 39 show the phase transformation of the Al_2O_3 composite sorbents under different conditions. It is shown that the freshly prepared composite sorbent is a mixture between Al_2O_3, $KAl(CO_3)_2*1.5H_2O$, and $K_2CO_3*1.5H_2O$, which confirms the formation of $KAl(CO_3)_2*1.5H_2O$ at 100^oC. The sample was then undergone a chemisorption of carbon dioxide in a presence of water. The carbon dioxide adsorption results in a chemical transformation of $K_2CO_3*1.5H_2O$ to $KHCO_3$ as shown in the presence of $KHCO_3$ reflections. The reaction takes place as follows:

$2K_2CO_3*1.5H_2O + 2CO_2 \Leftrightarrow 4KHCO_3 + 0.5H_2O$

The sample was then undergone a regeneration using steam at 150^oC for two hours. The XRD result shows reflection of $K_2CO_3*1.5H_2O$ indicating that $K_2CO_3*1.5H_2O$ is partially restored; however, no change in $KAl(CO_3)_2*1.5H_2O$ was observed. The DSC analyses was then utilized to investigate the stability of $KAl(CO_3)_2*1.5H_2O$.

The DSC spectra of K_2CO_3 samples exhibit many exothermic reactions between 50 and 500^oC. The intensity of these exothermic peaks increases as a function of the K_2CO_3 loading as shown in Figure 39. An exothermic peak between 175 and 200^oC shifted to higher temperature as K_2CO_3 loading increases. The sample of 50 wt.% K_2CO_3 was then selected and calcined at four temperatures (100^oC, 130^oC, 175^oC, 250^oC, and 400^oC). These samples were then analyzed by XRD to identify the phase of the compound as shown in Figure 40.

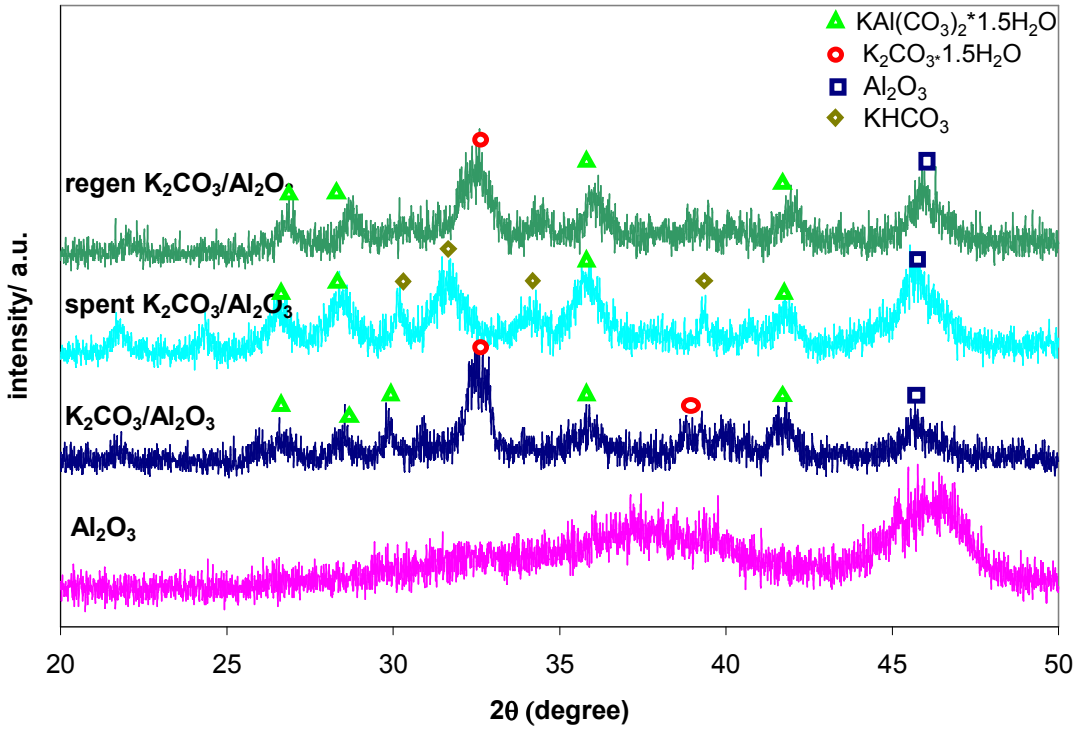

Figure 39: XRD patterns of Al_2O_3-composite sorbents under adsorption and regeneration

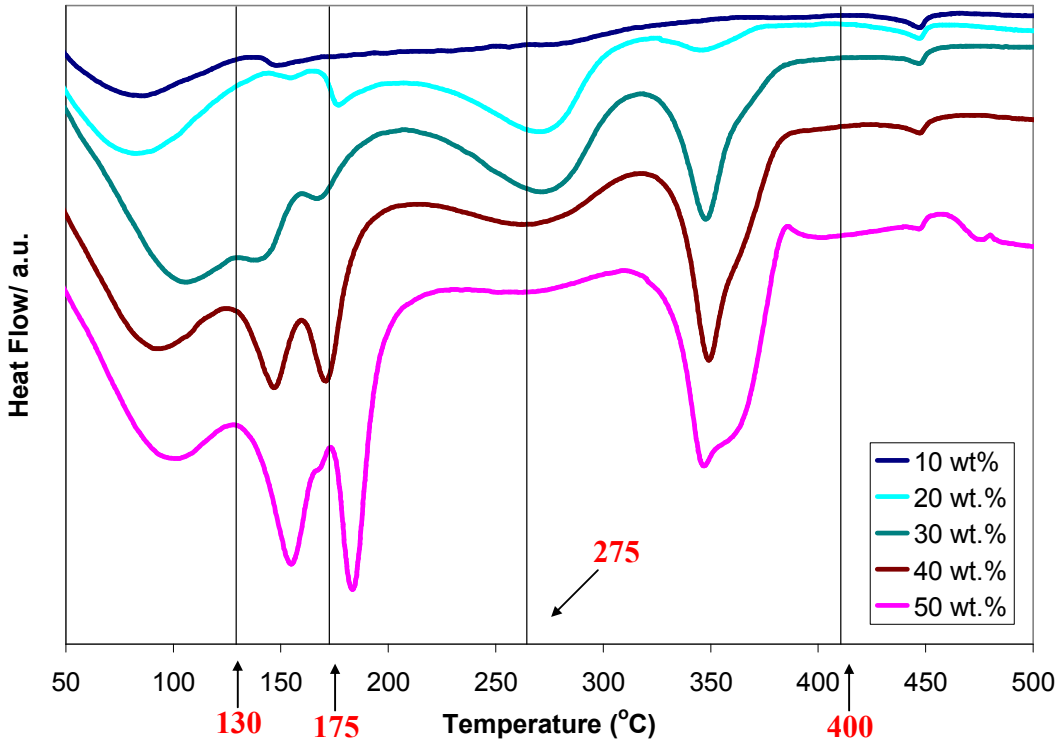

Figure 40: DSC spectra of spent K_2CO_3/Al_2O_3 at different K_2CO_3 loadings

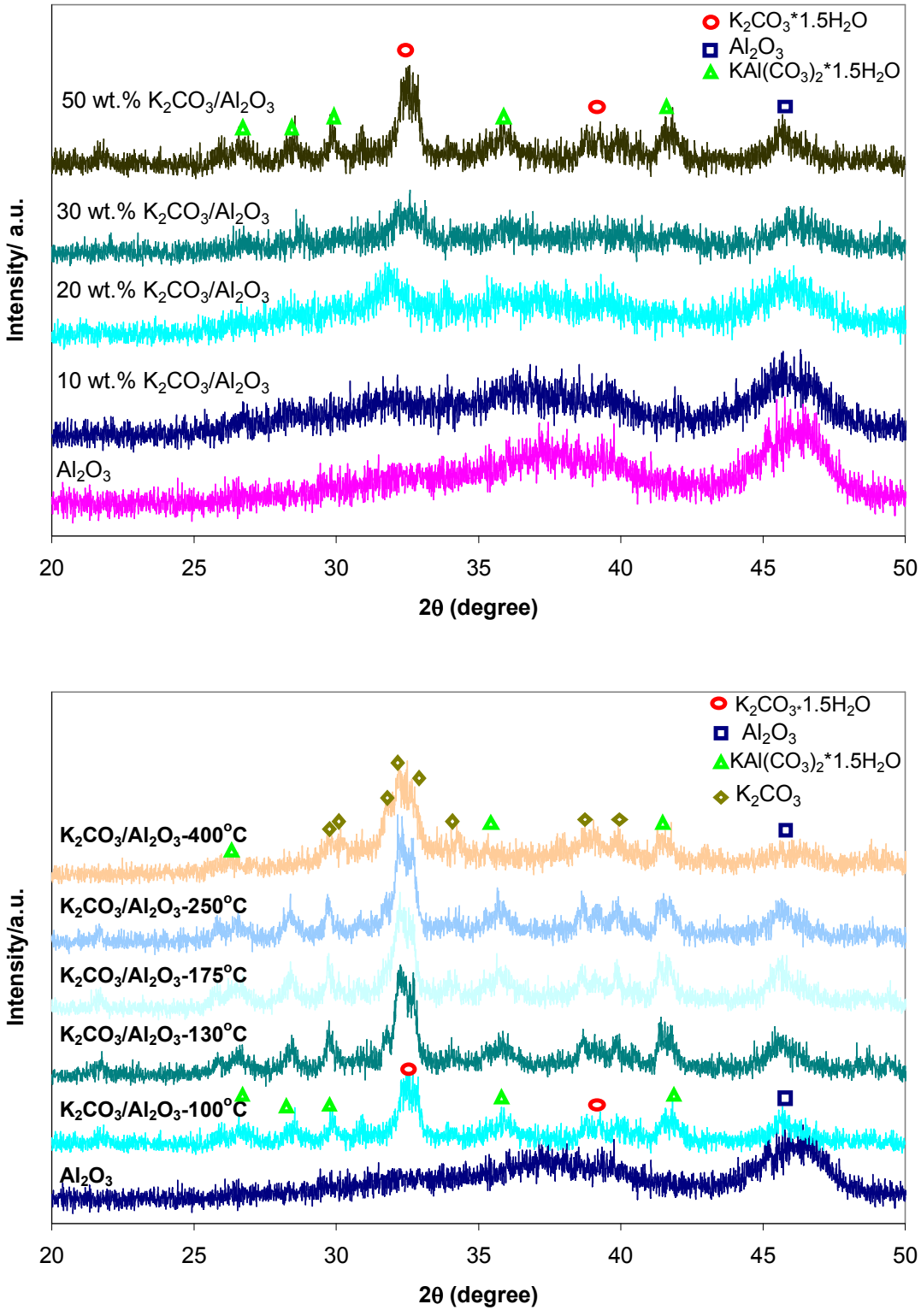

Figure 41: XRD patterns of K_2CO_3/Al_2O_3 calcined at different temperatures

Figure 41A shows the XRD patterns of Al_2O_3-composite sorbents at different K_2CO_3 loadings. At 5 wt.% K_2CO_3, the composite sorbent has the same feature as the Al_2O_3. The high pore volume of Al_2O_3 causes the high dispersion of K_2CO_3 in the pores. As a result, the formation of $KAl(CO_3)_2*1.5H_2O$ was not detected at low K_2CO_3 loading. Addition of K_2CO_3 enhances $KAl(CO_3)_2*1.5H_2O$ formation, which in turns reduces the pore volume and results in precipitation of $K_2CO_3*1.5H_2O$ as seen in the $K_2CO_3*1.5H_2O$ reflections at 20, 30, and 50 wt.% K_2CO_3. Due to the distinct phase identification, the Al_2O_3 composite sorbent with 50 wt.% K_2CO_3 was then utilized to calcined at 100^oC, 130^oC, 175^oC, and 350^oC show a mixture of Al_2O_3, potassium sesquihydrate, potassium alumino carbonate, and potassium carbonate. It was found that $K_2CO_3*1.5H_2O$ starts to lose its crystallization water at the temperature higher than 100^oC forming K_2CO_3. However, there is no change in $KAl(CO_3)_2*1.5H_2O$ reflections indicative of stability at elevated temperatures.

Summary

Even though alumina composite sorbents are not regenerated, they offer high carbon dioxide adsorption capacity, which can be used in the single-use gas purification process where molecular sieves are not possible due to the high humidity of the gas phase. However, a further investigation is needed for the alumina composite sorbents to gain a better understanding of the phase transformation and distribution in the porous alumina matrix as well as the reactions at elevated temperature to stabilize the formation of potassium alumino carbonate, which is inactive.

VII. CONCLUSIONS

The new regenerable sorbent has been developed for low carbon dioxide concentration removal applications at room temperature, such as in Metal-air batteries, Alkaline Fuel Cells, and air-purifying respirators for medical and military purposes. The breakthrough tests show that the nature of support materials has a strong influence on the CO_2 adsorption capacity in the sequence: SiO_2<ACP<Al_2O_3. The hydrothermal reaction between SiO_2 and Al_2O_3 and K_2CO_3 takes place during sorbent preparation forming inactive materials of potassium alumino silicate and potassium alumino carbonate respectively. However, an increase in K_2CO_3 loading causes the K^+ cations to diffuse into the lattice of Al_2O_3 forming potassium alumino carbonate. An increase in potassium alumino carbonate causes the precipitation of K_2CO_3*1.5H_2O, which readily reacts with carbon dioxide as shown in an increase in the carbon dioxide adsorption capacity. The regeneration of the Al_2O_3 composite sorbents is not possible, whereas the ACP composite sorbents can be regenerated reversibly. The K_2CO_3/ACP sorbents were stable in cyclic adsorption/regeneration cycles and recovered 98% CO_2 adsorption capacity under regeneration in steam at 150^oC for two hours.

The microfibrous entrapped K_2CO_3/ACP sorbents were then developed. The use of microfibrous media reduces the effect of intraparticle diffusion and allows high

contacting efficiency while lowering the thermal effects and pressure drops. The breakthrough tests and structural analyses indicate that the microfibrous entrapped K_2CO_3/ACP sorbents are thermally stable and structurally robust in multicyclic breakthrough tests. This approach enhances the process intensification while reduces the adsorber mass and size.

REFERENCES

1. Friedlingstein, Pierre; Solomon, Susan., "Contributions of past and present human generations to committed warming caused by carbon dioxide," Proceedings of the National Academy of Sciences of the United States of America, Vol. 102(31), 2005, 10832-10836.

2. Wang, B., Jin, H., Zheng, D., "Recovery of CO_2 with MEA and K_2CO_3 absorption in the IGCC system," International Journal of Energy Research, Vol. 28, 2004, 521-535.

3. Fee, J. P. H., Murray,J. M., Luney,S. R, "Molecular sieves : an alternative method of carbon dioxide removal which does not generate compound A during simulated low-flow sevoflurane anaesthesia," Anaesthesia (Anaesthesia), Vol. 50, 1995, 841-845.

4. Robinson, A., Baliunas, S., SOON, W. and Robinson, Z., "Environmental Effects of Increased Atmospheric Carbon Dioxide," http://www.oism.org/pproject/s33p36.htm (This figure was created by Robert A. Rohde)

5. Xu, X., Song, C, Miller, B, and Scaroni, A.W., "Adsorption separation of carbon dioxide from flue gas of natural gas-fired boiler by a novel nanoporous "molecular basket" adsorbent," Fuel Processing Technology, Vol. xx, 2005, xxx-xxx.

6. Yong, Z., Mata, V.G., and Rodrigues, A.E., "Adsorption of carbon dioxide on chemically modified high surface area carbon-based adsorbents at high temperature," Adsorption, Vol.7, 41-50, 2001.

7. Luby, P., "Zero Carbon Power Generation: IGCC as the Premium Option," Petroleum and coal, Vol. 46(1), 2004, 1-16.

8. Sasaoka, E., "Characterization of Reaction between Zinc Oxide and Hydrogen Sulfide," Energy & Fuels, Vol. 8, 1994, 1100-1105.

9. Sasaoka, E., Taniguchi, K., Hirano, S., Uddin, Md. A., Kasaoka, S., and Sakata, Y., "Catalytic Activity of ZnS Formed from Desulfurization Sorbent ZnO for Conversion of COS to H_2S," Industrial Engineering & Chemistry Research, Vol. 34, 1995, 1102-1106.

10. Eckart, P., "Speaceflight Life Support and Biopherics," Kluwer Academic Publishers, 1996.

11. Web resources: http://www.eere.energy.gov/hydrogenandfuelcells/fuelcells/fc_types.html?print#comparison

12. Malone, E., Rasa, K., Cohen, D., Isaacson, T., Lashley, H., and Lipson, H., "Freeform fabrication of zinc-air batteries and electromechanical assemblies," Rapid Prototyping Journal, Vol. 10, 2004, 58-69.

13. Web resources: www.nexant.com

14. Lu, Y., Chen, S., Rostam-Abadi, M., Varagani, R., Chatel-Pelage, F., Pranda, P., Bose, A.," Techno-economic study of the oxy-combustion process for CO_2 capture from coal-fired power plants," Proceedings - Annual International Pittsburgh Coal Conference, 22nd, 2005, 277/1-277/15.

15. Koss, U., Meyer, M.," "Zero emission IGCC " with Rectisol Technology," Proceedings - Annual International Pittsburgh Coal Conference, 20th, 2000, 779-786.

16. Hochgesand, G., "Rectisol and Purisol," European and Japanese Chemical Industries Symposium, Vol.62 (7), 1970.

17. Fuertest, A.B., Alvarez, D., Rubiera, F., Pis, J.J., Palacios, J.M., "Surface area and pore size changes during sintering of calcium oxide particles," Chemical engineering Communications, vol. 109, 1991, 73-88.

18. Barker, R.S., Russel, M.R., and Whitmer, L.R., "Mathematical Modelling of a Four-Bed Molecular Sieves with CO_2 and H_2O Collection," SAE Technical Paper Series No. 911470, 21st International Conference on Environmental Systems, San Francisco, CA, July 15-18, 1991.

19. Web resources:
http://www.sigmaaldrich.com/Brands/Aldrich/Tech_Bulletins/AL_143/Molecular_Sieves.html

20. Tatarchuk, B. J., Rose, M. F., Krishnagopalan, A., Zabasajja, J.N., Kohler, D., US Patent 5,304,330, 1994; US Patent 5,080,963, 1992.

21. Overbeek, R. A., Khonsari, A. M., Chang, Y.-F., Murrell, L. L., Tatarchuk, B. J., Meffert, M. W., US Patent 6,231,792, 2001.

22. Tatarchuk, B. J. US Patent 5,096,663, 1992; US Patent 5,102,745, 1992.

23. Zhang, L., Lin, J., Chen, Y., " A Study of the Interaction of Li_2O and γ-Al_2O_3," Journal of solid state chemistry, Vol. 97, 1992, 292-298

24. Cahela, D. R., and Tatarchuk, B. J., "Design of Polishing Filter Adsorbents Using Sintered Microfibrous Metallic Networks as Carriers for High Effectiveness Sorbent Particulates." Proceedings of the AIChE 2003 Annual Meeting: Fundamentals of Adsorption and Ion Exchange II. San Francisco, CA, Nov. 16 – 21, 2003.

25. Meffert, M. W., "Preparation and Characterization of Sintered Metal Microfiber-Based Composite Materials for Heterogeneous Catalyst Applications," Dissertation, Auburn University, 1998.

26. Crittenden, B. and Thomas, W. J., "Adsorption Technology & Design," Woburn: Butterworth Heinemann, 1998.

27. Noll, K., Gounaris, V., Hou, W., "Adsorption Techonology for Air and Water Pollution Control," Lewis Publishers, Inc., 1992.

28. Bohart, G. S. and Adams, E. Q., "Some Aspects of the Behavior of Charcoal with Respect of Chlorine," Journal of American Chemical Society, Vol. 42, 1920, 530.

29. Cahela, D. R., and Tatarchuk, B.J., "Permeability of Sintered Microfibrous Composites for Heterogeneous Catalysis and Other Chemical Processing Opportunities," Catalysis Today, Vol. 69, 2001, 33-39.

30. Yoon, Y. and Nelson, J., "Application of Gas Adsorption Kinetics I. A Theoretical Model for Respirator Cartridge Service Life," American Industrial Hygiene Association Journal, Vol. 48, 1984, 509-516.

31. Chang, B.K. and Tatarchuk, B.J., " Microfibrous Entrapment of Small Catalyst Particulates for High Contacting Efficiency Removal of Trace CO from Practical Reformates for PEM H_2-O_2 Fuel Cells," Journal of Materials Engineering and Performance, Vol.15, 2006, 453-456

32. Chang, B.K., Lu, Y., Yang, H., Tatarchuk, B.J., "Facile Regeneration Vitreous Microfibrous Entrapped Supported ZnO Sorbents with High Contacting Efficiency for Bulk H_2S Removal from Reformate Streams in Fuel Cell Applications," Journal of Materials Engineering and Performance, Vol.15, 2006, 439-441

33. Yang, H. Y.; Sathitsuksanoh, N.; Lu, Y.; Tartarchuk, B. J., "Moderate temperature H_2S removal over high specific surface area SiO_2 supported ZnO sorbent: Design and preparation," AIChE Annual Meeting, Conference Proceedings, Cincinnati, OH, United States, Oct. 30-Nov. 4, 2005.

34. Okunev, A.G., Sharonov, V.E., Aristov, Y.I., Parmon, V.N., "Sorption of carbon dioxide from wet gases by K_2CO_3-in-porous matrix," React.Kinet.Catal.Lett., Vol.71(2), 355-362, 2000.

35. Sharonov, V.E., Tyshchishchin, E.A., Moroz, E.M., Okunev, A.G., and Aristov, Y.I., "Sorption of CO_2 from humid gases on potassium carbonate supported by porous matrix," Russian Journal of Applied Chemistry, Vol. 74(3), 2001, 409-413.

36. Roine, A., “HSC Chemistry for Windows,” Version 4.0, Outokumpu Research Oy, Pori, Finland, 1999.

37. Deshpande, D.A., Ghormare, K.R., Deshpande, N.D., Tankhiwale, A.V., “Dehydration of Crystalline K_2CO_3*1.5H_2O,” Thermochica Acta, Vol. 66, 1983, 255-265.

38. Klos, I. And Klos, R., “Polish Soda Lime in Military Application,” Oswiecim, 2004.